UNIVERSIDAD NACIONAL AUTÓNOMA DE MÉXICO

PROGRAMA DE POSGRADO EN CIENCIAS FÍSICAS
FACULTAD DE CIENCIAS
MATERIA CONDENSADA Y NANOCIENCIAS

A DIVIDE-AND-CONQUER ALGORITHM BASED ON S-MATRICES: CONDUCTANCE IN RANDOMLY CONNECTED NANOSTRUCTURES

TESIS
QUE PARA OPTAR POR EL GRADO DE:
MAESTRO EN CIENCIAS (FÍSICA)

PRESENTA:
MAURICIO JAVIER RODRÍGUEZ GARCÍA

Dr. CARLOS RAMIREZ RAMOS
FACULTAD DE CIENCIAS
Dr. RAÚL PATRICIO ESQUIVEL SIRVENT
INSTITUTO DE FÍSICA
Dr. LUIS ANTONIO PÉREZ LÓPEZ
INSTITUTO DE FÍSICA

CIUDAD UNIVERSITARIA, CD. MX., ENERO, 2023

Acknowledgments

Words cannot express my gratitude to the chair of my committee, *Dr. Carlos Ramírez Ramos*, for the guidance, support, and motivation provided during all these years of work. I am also thankful to the rest of my committee, *Dr. Raúl Patricio Esquivel Sirvent* and *Dr. Luis Antonio Pérez López*, for their insightful comments that greatly improved the outcome of this work. Additionally, I am extremely grateful to the Consejo Nacional de Ciencia y Tecnología (CONACYT) for the financial aid provided during my two years of study. Even more, this research was accomplished thanks to the Programa de Apoyo a Proyectos de Investigación e Innovación Tecnológica (PAPIIT) de la UNAM IN109022, and all the computations presented in this work were performed at Miztli supercomputer under project LANCAD-UNAM-DGTIC-329.

I am also grateful to my parents and sisters for all the love and support they always give me. Thanks should also go to *Gustavo, Yael, Martín,* and *Jazmin* for all the laughs, experiences, and inspiring conversations, which I truly treasure. Lastly, I would be remiss in not mentioning *Mario* and *Miguel*. Their belief in me and all the stress relieved during our game nights helped me maintain my motivation during this process.

Contents

Abstract

In this work, the Landauer conductance of various random networks is computed via the implementation of a Divide-and-Conquer algorithm based on the Recursive Scattering Matrix Method (RSMM). Firstly, a brief introduction to the handled terminology, the Landauer conductance, the Scattering matrix theory, and the tight-binding approximation is provided. Then, the principle of the RSMM is presented along with its building blocks. Next, the Divide-and-Conquer algorithm is explained, and its computational complexity is analyzed. Obtaining that it makes the computational scaling of the RSMM smaller than the one of other state-of-the-art recursive methods. Finally, the conductance of the Erdös-Rényi, the Small World, and the Scale Free networks is presented for two cases: the links in the network are simply atomic bonds, and the links consist of one-dimensional periodic chains. Obtaining different characteristic behaviors for each case and network.

1. Landauer conductance

Electronic transport in the mesoscopic scale was first studied under the scope of scattering theory by Rolf Landauer [1,2]. This approach relates the conduction properties of a junction and the probability that an electron can be transmitted through it [3,4], and is valid when particle interactions are negligible and the transport is coherent. However, it is also applicable to incoherent transport if the vertical flow of electrons, *i.e.*, the flow from one energy channel to another, can be neglected.

The simplicity of this approach facilitated the study of the conductance in nanojunctions and led to further developments in this area [5–11]; and given its generality, it is considered to be the base of our understanding of electronic transport. A full review on this topic is given in Ref. [12].

In the following, the terminology that is used throughout this work is stablished; then, a heuristic derivation of the Landauer formula based on Refs. [3,4,13] is provided; later, the scattering and transfer matrices and their relation to the Landauer conductance is introduced; and lastly, the tight-binding approximation is briefly explained, since it is the physical model of this work.

1.1 Terminology and concepts

The approach in this work is for quasi-one-dimensional systems at zero temperature. These systems are quantum junctions that we can divide in three parts as shown in Fig. 1.1: Electrodes, leads, and scattering region (or scatterer).

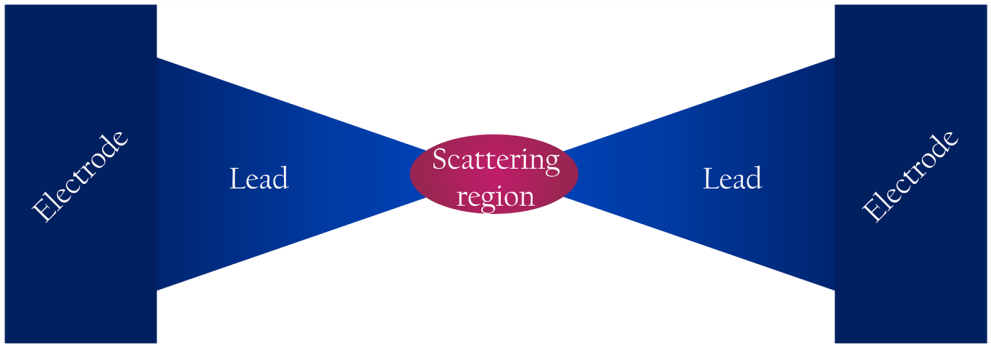

Figure 1.1.- Scheme of a quasi-one-dimensional junction. The leads connect the scattering region to the electrodes.

The electrodes are the regions where the electrons are incoherent and in equilibrium, therefore, any electron that enters them is thermalized and loses any phase information it had. Additionally, we assume them to be reflectionless, which means that every electron that strikes the electrode will enter it.

The central region is made up of the leads and the scattering region. Here, the transport is coherent, and the particles do not interact with each other. The leads are the regions that connect the electrodes to the scatterer and consist of ballistic conductors that have a well-defined mode structure, which are $\psi_n^{(\pm)}$ and $\varphi_m^{(\pm)}$ for the left and right lead respectively, where the plus sign denotes the modes traveling towards the scattering region, and the minus sign corresponds to the modes traveling away from it. On the other hand, the scattering region is any given mesoscopic system under study, it has the property of being able to reflect the particles back to the lead from where they are arriving, or to transmit them into the other lead. In other words, each electron has a probability $T_{n,m}(E)$ of being transmitted from the n-th mode of one lead, through the scatterer, into the m-th mode of the other lead, where E is the particle's energy.

Now, it is assumed that the leads provide an adiabatic connection between the electrodes and the scattering region, this means that the infinite number of modes in the electrodes decreases adiabatically until reaching the scatterer. This implies that if an electron with energy E strikes the lead, then the leads' propagation modes can either fully transmit it, open channels, or fully reflect it, closed channels.

1.2 A derivation of the Landauer formula

Let us start by analyzing an energy diagram, shown in Fig. 1.2, of the junction presented in Fig. 1.1. The electrode to the left (right) of the scatterer, electrode L (R), has chemical potential μ_L (μ_R); where it is considered that $\mu_L - \mu_R = eV$ with e the elemental charge, and V a small external voltage. And ϕ_s^α, with $s = L, R$ and $\alpha = +, -$, represents a particle originated in electrode s traveling towards the scattering region, $\alpha = +$, or away from it, $\alpha = -$.

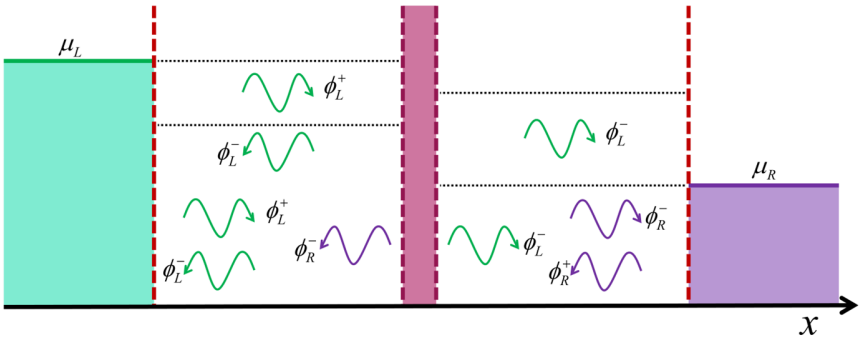

Figure 1.2.- Energy diagram of particles moving in a quantum junction.

Now, the total current can be expressed in terms of the net flow of electrons in the system, which has to account for all the transmissions between channels, as

$$I = \frac{e}{h}\sum_{n,m}\int_{-\infty}^{\infty} T_{n,m}(E)\left[f(E,\mu_L) - f(E,\mu_R)\right]dE\,, \tag{1.1}$$

where the spin degeneracy is being ignored. Notice that the particles generated in electrode s follow its energy distribution $f(E,\mu_s)$, which in general is the Fermi distribution; however, we are in the zero-temperature scenario, so the energy distribution corresponds instead to the Heaviside's step function, *i.e.*,

$$f(E,\mu_s) = \Theta(\mu_s - E) = \begin{cases} 1, & E < \mu_s \\ 0, & E \geq \mu_s \end{cases}. \tag{1.2}$$

After substituting Eq. (1.2) into Eq. (1.1), one gets

$$\begin{aligned} I \quad &= \frac{e}{h}\sum_{n,m}\int_{-\infty}^{\infty} T_{n,m}(E)\left[\Theta(\mu_L - E) - \Theta(\mu_R - E)\right]dE \\ &= \frac{e}{h}\sum_{n,m}\int_{\mu_R}^{\mu_L} T_{n,m}(E)dE \\ &= \frac{e}{h}\int_{\mu_R}^{\mu_L} T(E)dE \\ &= \frac{e^2}{h}T(E_F)V, \end{aligned} \tag{1.3}$$

where $T(E) = \sum_{n,m} T_{n,m}(E)$ is the *transmission function*, and to solve the integral, the external voltage is considered to be small enough so that $T(E) = T(E_F)$, with E_F the

Fermi energy, in the energy interval $[\mu_R, \mu_L]$. Lastly, given that the conductance, G, satisfies $I = GV$, Eq. (1.3) leads to what is known as Landauer's second formula:

$$G = \frac{e^2}{h} T \,. \tag{1.4}$$

It is also worth mentioning the existence of Landauer's first formula,

$$G = \frac{e^2}{h} \frac{T}{1-T} \,. \tag{1.5}$$

These two formulas are equally valid, but they refer to the conductance between different sets of point inside the same system. Following the scheme in Fig. 1.3, Eq. (1.4) refers to the conductance between L and R. That is why even for a perfect wire, $T = 1$, there exists a finite conductance e^2/h; this is due to the contact resistance between the electrode and the lead since there is a jump from an effectively infinite number of modes in the electrode to a finite number of them in the lead.

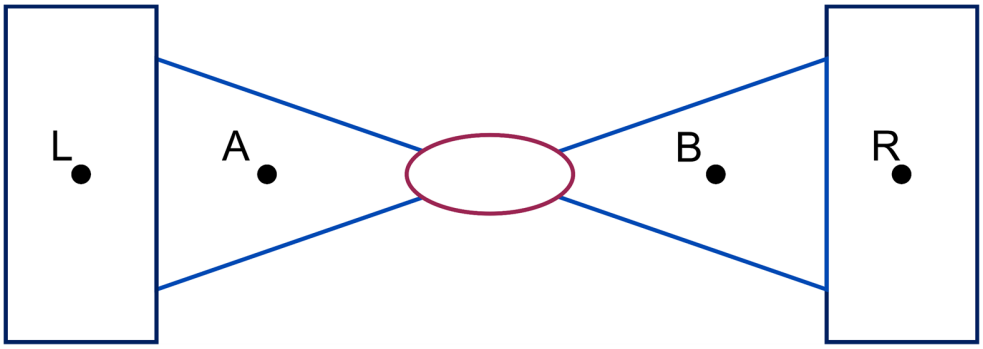

Figure 1.3.- Sets of points of voltage measurements. A and B inside the leads, and L and R inside the electrodes.

On the other hand, Eq. (1.5) corresponds to the conductance between A and B. Notice that, in this case, the conductance of a perfect wire does go to infinity, as expected due to the lack of resistances in the system. A more thorough explanation of the difference between both Landauer's formulas can be found in Ref. [14].

1.3 Scattering and transfer matrices

Let us now consider that the left (right) lead has $\{\psi_n^{(\pm)}\}$ ($\{\varphi_m^{(\pm)}\}$) modes with $\{A_n^{(\pm)}\}$ ($\{B_m^{(\pm)}\}$) related amplitudes; where the $\pm$ represents that the particle travels

towards, $+$, or away from, $-$, the scattering region. These amplitudes of incoming and outgoing waves are related by the scattering matrix (S-matrix) of the system, $\mathbf{S}$, as

$$\begin{pmatrix} A_1^{(-)} \\ \vdots \\ A_N^{(-)} \\ B_1^{(-)} \\ \vdots \\ B_M^{(-)} \end{pmatrix} = \overbrace{\begin{pmatrix} \mathbf{r} & \mathbf{t}' \\ \mathbf{t} & \mathbf{r}' \end{pmatrix}}^{\mathbf{S}} \begin{pmatrix} A_1^{(+)} \\ \vdots \\ A_N^{(+)} \\ B_1^{(+)} \\ \vdots \\ B_M^{(+)} \end{pmatrix}, \tag{1.6}$$

where the matrices $\mathbf{r}$ ($N \times N$) and $\mathbf{t}$ ($M \times N$) describe the reflection and transmission of waves incoming from the left lead, and the matrices $\mathbf{r}'$ ($M \times M$) and $\mathbf{t}'$ ($N \times M$) do the same for waves incoming from the right one.

On the other hand, in case that $N = M$, it is possible to solve the problem using the transfer matrix of the system, $\mathbf{M}$, which relates the left amplitudes with the right amplitudes as

$$\begin{pmatrix} A_1^{(+)} \\ \vdots \\ A_N^{(+)} \\ A_1^{(-)} \\ \vdots \\ A_N^{(-)} \end{pmatrix} = \overbrace{\begin{pmatrix} \mathbf{M}_{11} & \mathbf{M}_{12} \\ \mathbf{M}_{21} & \mathbf{M}_{22} \end{pmatrix}}^{\mathbf{M}} \begin{pmatrix} B_1^{(+)} \\ \vdots \\ B_N^{(+)} \\ B_1^{(-)} \\ \vdots \\ B_N^{(-)} \end{pmatrix}. \tag{1.7}$$

If we think of the system as made up by J different consecutive subsystems or layers, where subsystem i has an associated transfer matrix, $\tilde{\mathbf{M}}_i$, that stablishes how the waves' amplitudes change after traversing the i-th layer of the system, then the transfer matrix of the whole system is given by

$$\mathbf{M} = \tilde{\mathbf{M}}_1 \tilde{\mathbf{M}}_2 \cdots \tilde{\mathbf{M}}_J, \tag{1.8}$$

where the layers are enumerated from left to right and their associated transfer matrices are square matrices of the same dimension [3].

Now, since the interest is to determine the transmission of the system from left to right, the amplitudes $\{B_m^{(+)}\}$ can be set to zero, obtaining

$$\begin{pmatrix} A_1^{(+)} \\ \vdots \\ A_N^{(+)} \end{pmatrix} = \mathbf{M}_{12} \begin{pmatrix} B_1^{(-)} \\ \vdots \\ B_M^{(-)} \end{pmatrix}. \tag{1.9}$$

This consideration can be applied to Eq. (1.6), resulting in

$$\begin{pmatrix} B_1^{(-)} \\ \vdots \\ B_M^{(-)} \end{pmatrix} = \mathbf{t} \begin{pmatrix} A_1^{(+)} \\ \vdots \\ A_N^{(+)} \end{pmatrix}, \tag{1.10}$$

which leads to the relation

$$\mathbf{t} = \mathbf{M}_{12}^{-1}. \tag{1.11}$$

The $\mathbf{t}$ matrix is called *transmission matrix*, and its entries satisfy the relation $T_{mn} = |\mathbf{t}_{mn}|^2$. Therefore, considering the fact that

$$\sum_{n=1}^{N}\sum_{m=1}^{M} T_{mn} = \sum_{n=1}^{N}\sum_{m=1}^{M} \mathbf{t}_{mn}\mathbf{t}^{\dagger}{}_{nm} = \sum_{n=1}^{N} (\mathbf{t}\mathbf{t}^{\dagger})_{nn} = \mathrm{Tr}(\mathbf{t}\mathbf{t}^{\dagger}), \tag{1.12}$$

the transmission function is given by $T(E) = \mathrm{Tr}(\mathbf{t}\mathbf{t}^{\dagger})$, and the second Landauer's formula is generalized to

$$G = \frac{e^2}{h}\mathrm{Tr}(\mathbf{t}\mathbf{t}^{\dagger}). \tag{1.13}$$

A more thorough analysis of this case is performed in Ref. [15].

1.4 Tight-binding approximation

This approach consists in taking a system made up of atoms and supposing that their electrons are strongly attached to them; that is, each molecular orbital is effectively localized giving place to short range interactions. Therefore, when an electron enters the system, it will only be able to move from one atom to another if there is an interaction between their orbitals.

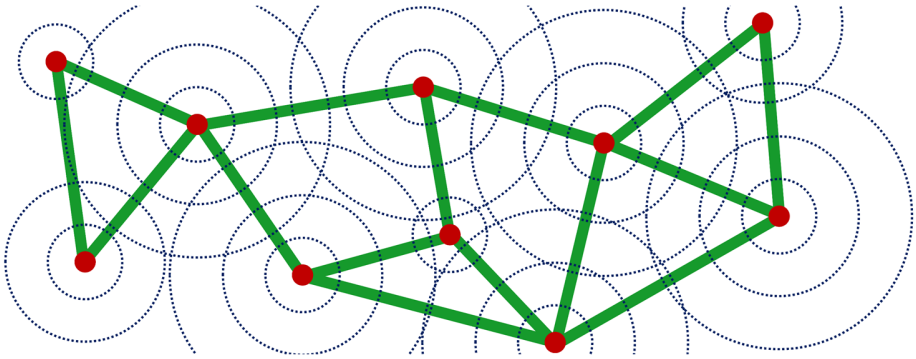

Figure 1.4.- Scheme of a tight binding system of $N = 10$ atoms (red circles) where each has up to three orbitals (dotted circles). The interaction between two atoms is represented by a green line.

To make things clearer, let us consider a system of N atoms (also called *sites*) where atom n has P_n orbitals, like the one shown in Fig. 1.4, where the interaction between two atoms is represented by a solid green line regardless of the number of orbitals that are interacting to illustrate the short range assumption. Using Dirac's notation, we can define the p-th orbital of the n-th atom as $|\phi_{n,p}\rangle$, where the order of numeration is arbitrary. These are the localized functions for atomic orbitals; however, they are not necessarily orthogonal to each other. Therefore, it is preferable to utilize the Wannier functions, who are orthonormal and will be denoted as $|n,p\rangle$.

Now, the Hamiltonian of this system can be written as

$$\hat{H} = \sum_{n=1}^{N}\sum_{p=1}^{P_n} \varepsilon_{n,p} |n,p\rangle\langle n,p| + \sum_{n=1}^{N}\sum_{p=1}^{P_n}\sum_{\substack{m=1 \\ m\neq n}}^{M}\sum_{q=1}^{P_m}\left[t_{n,p,m,q} |n,p\rangle\langle m,q| + t^{*}_{n,p,m,q} |m,q\rangle\langle n,p| \right], \qquad (1.14)$$

where $\varepsilon_{n,p}$ is called the *on-site energy* since it is the energy that a particle would have if it were only in state $|n,p\rangle$, and $t_{n,p,m,q}$ is called the *hopping parameter* since its module is proportional to the probability of an electron jumping from state $|m,q\rangle$ into state $|n,p\rangle$ with $m \neq n$. The hopping parameters are complex numbers in general, but they are real numbers in the time-reversal case.

This model allows us to calculate the particle's wave functions in the system. So, one can compute the system's S-matrix under this model as explained in the next chapter.

As final remarks, in this work the time-reversal case for quasi-one-dimensional junctions at zero temperature under the tight binding approximation with only one orbital per site is considered. Also, since the scattering region must be far away from the electrodes, so they do not interact with the scatterer, the common assumption of the leads being semi-infinite periodic structures is also considered and the electrodes are disregarded.

2. Recursive Scattering Matrix Method (RSMM)

When computing the conductance of a physical system, we come to the realization that there is a small number of systems that can be analytically solved. Therefore, we turn to numerical simulations and computational algorithms to be able to solve more complex systems.

The most usual methods to do this are the Green function method [16,17] and the transfer matrix method [3,4]. However, in the most recent years, there have been advancements in methods that utilize the S-matrix of the system, like the Kwant software, which operates by utilizing sparse matrix diagonalization techniques [18], and the RSMM [19]. The latter presents a number of operations and a memory usage comparable to those of Recursive Green Function (RGF) methods. It also shows a fast calculation of transport properties, total density of states, and other physical quantities. Additionally, the S-matrix approach does not require to consider a finite imaginary part of the energy, which improves accuracy compared to RGF methods.

In this chapter, I explain the basics and the operation of the RSMM to lay the foundations for the detailed implementation in the next chapter.

2.1 Constructing a system

The RSMM's principle is that if one has the S-matrices of two systems, A and B, that are attached to periodic 1D-chains of null site energy and hopping parameter t_C, then one can glue these systems together and obtain the S-matrix of the resulting system C.

Now, let us consider an arbitrary tight-binding system, for example, one of the shown in Fig. 2.1, where the red circles represent the sites with their respective on-site energies, the dark purple solid lines represent the interactions with their respective hopping parameters, and the dot-dashed purple lines represent 1D semi-infinite periodic chains of parameter t_C. These 1D chains are also called *auxiliary chains* since they strictly are not part of the scattering region.

These auxiliary chains can be considered as the leads of the system, since they are semi-infinite and periodic, but they can also serve another purpose. As

explained in the previous chapter, the S-matrix relates the amplitudes of incoming waves into a system with those of the outgoing waves from it, therefore, these waves need a way to reach and leave the system, and the auxiliary chains provide it, which leads to the fact that the dimension of the S-matrix of the system is equal to the total number of chains attached to it. 1D-chains are an optimal choice since they only have one channel, and they allow us to glue two systems together.

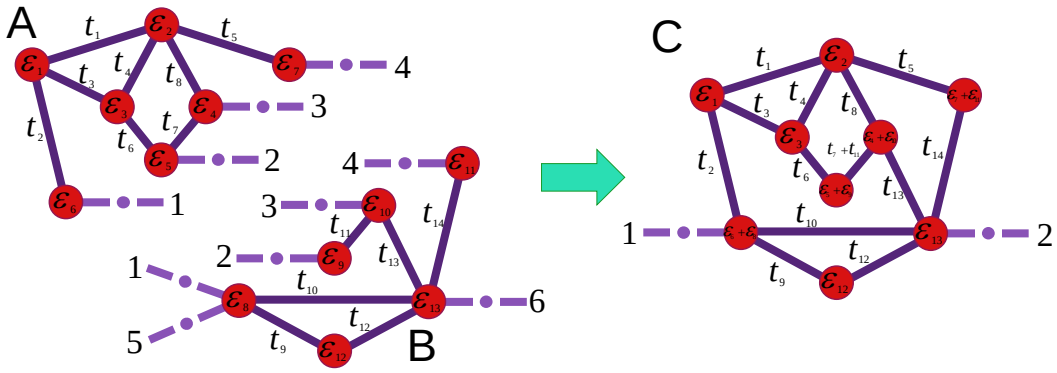

Figure 2.1.- Gluing process operation diagram. The wave amplitudes of the first four auxiliary chains of structures A and B are equated to obtain structure C. On-site energies and hopping parameters that overlap are added. The remaining chains are renumbered.

Using the scheme shown in Fig. 2.1 as reference, if one wants to glue together systems A and B to obtain C, then one must equate the incoming (outgoing) wave's amplitude of system A, $A^{(+)}$ ($A^{(-)}$), to the outgoing (incoming) wave's amplitude of system B, $B^{(-)}$ ($B^{(+)}$), but only for the chains attached to the sites that are being fused together. Following the example, to obtain system C one must equate

$$A_i^{(\pm)} = B_i^{(\mp)} \quad \text{for} \quad i = 1,2,3,4, \tag{2.1}$$

where the subindex refers to the number of auxiliary chains of the system, so the site of A that is attached to auxiliary chain i is being fused to the site of B that is attached to auxiliary chain i. Notice that this gluing process adds together the on-site energies and hopping parameters that overlap, it also makes disappear the auxiliary chains that are attached to the sites being fused. Consequently, an important consideration when gluing two systems together is that the resulting structure must have at least one remaining 1D-chain so that its S-matrix exists.

In a general case, consider that system A is attached to M_A auxiliary chains and system B is attached to M_B auxiliary chains, and N chains of each are glued together to form system C. Since the enumeration of the chains is arbitrary, we can assume that the first N chains of each system are the ones attached to the sites being fused, as in the previous example. This allows us to write the S-matrices of A and B as

$$\mathbf{S}^{A/B} = \begin{pmatrix} \mathbf{S}_{11}^{A/B} & \mathbf{S}_{12}^{A/B} \\ \mathbf{S}_{21}^{A/B} & \mathbf{S}_{22}^{A/B} \end{pmatrix}, \tag{2.2}$$

where $\mathbf{S}_{11}^{A}$ ($\mathbf{S}_{11}^{B}$) is an $N \times N$ matrix that corresponds to the scattering of incoming waves through the first N chains into the same chains for system A (B); $\mathbf{S}_{12}^{A}$ ($\mathbf{S}_{12}^{B}$) is a $N \times [M_A - N]$ ($N \times [M_B - N]$) matrix that relates the amplitudes of incoming waves through the last $M_A - N$ ($M_B - N$) chains to the ones outgoing from the first N chains of system A (B); $\mathbf{S}_{21}^{A}$ ($\mathbf{S}_{21}^{B}$) is a $[M_A - N] \times N$ ($[M_B - N] \times N$) matrix that relates the amplitudes of incoming waves through the first N chains to the ones outgoing from the last $M_A - N$ ($M_B - N$) chains of system A (B); and, $\mathbf{S}_{22}^{A}$ ($\mathbf{S}_{22}^{B}$) is an $[M_A - N] \times [M_A - N]$ ($[M_B - N] \times [M_B - N]$) matrix that corresponds to the scattering of the incoming waves through the last $M_A - N$ ($M_B - N$) chains into themselves for system A (B).

Equation (2.2) lets us write the S-matrix of the resulting system C, $\mathbf{S}^{C}$, as [19]

$$\mathbf{S}^{C} = \begin{pmatrix} \mathbf{S}_{22}^{A} + \mathbf{S}_{21}^{A}\left(\mathbf{I} - \mathbf{S}_{11}^{B}\mathbf{S}_{11}^{A}\right)^{-1}\mathbf{S}_{11}^{B}\mathbf{S}_{12}^{A} & \mathbf{S}_{21}^{A}\left(\mathbf{I} - \mathbf{S}_{11}^{B}\mathbf{S}_{11}^{A}\right)^{-1}\mathbf{S}_{12}^{B} \\ \mathbf{S}_{21}^{B}\left(\mathbf{I} - \mathbf{S}_{11}^{A}\mathbf{S}_{11}^{B}\right)^{-1}\mathbf{S}_{12}^{A} & \mathbf{S}_{22}^{B} + \mathbf{S}_{21}^{B}\left(\mathbf{I} - \mathbf{S}_{11}^{A}\mathbf{S}_{11}^{B}\right)^{-1}\mathbf{S}_{11}^{A}\mathbf{S}_{12}^{B} \end{pmatrix}. \tag{2.3}$$

Obtaining a recipe to compute the S-matrix of any tight-binding system if we know the S-matrices of two of its subsystems that can generate it by being glued together. Notice that these two subsystems are not unique, and their choice can greatly impact the computational scaling of this algorithm's implementation. This remark is analyzed in more depth in the next chapter.

2.2 Building blocks

Now that the gluing process has been stablished, it is important to highlight the essential systems for this method, which are called *building blocks* since one can build any given structure with only these systems just by iteratively gluing them.

These building blocks are shown in Fig. 2.2 and consist of (a) a single site of energy ε attached to p auxiliary chains (represented by purple dot-dashed lines), and (b) two sites of null energy attached by a bond of hopping parameter t (represented by a dark purple solid line) and each site is connected to one auxiliary chain.

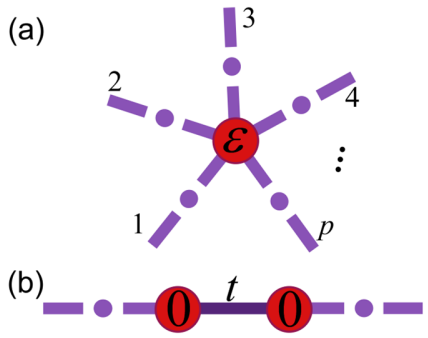

Figure 2.2.- Building blocks of the RSMM. (a) Site of energy ε attached to p auxiliary chains. (b) Bond of hopping parameter t between two sites of null energies.

The corresponding S-matrices of these site and bond structures are [19]

$$\left[\mathbf{S}^{\text{site}}\right]_{nm} = \frac{2it_C \sin\kappa}{\varepsilon - E + t_C e^{i\kappa} p} - \delta_{nm},$$
$$\left[\mathbf{S}^{\text{bond}}\right]_{nm} = \begin{cases} r & \text{if } n = m \\ \frac{t_C}{t}(e^{i\kappa} + re^{-i\kappa}) & \text{if } n \neq m, \end{cases} \tag{2.4}$$

where $\mathbf{S}^{\text{site}}$ is a $p \times p$ matrix, $\mathbf{S}^{\text{bond}}$ is a 2×2 matrix, E is the energy of the particle that enters the system,

$$\kappa = \cos^{-1}\left(\frac{E}{2t_C}\right) \in [0, \pi], \tag{2.5}$$

and

$$r = -\frac{t^2 - t_C^2}{t^2 - t_C^2 e^{-2i\kappa}}. \tag{2.6}$$

The wave number κ is dimensionless since the distance between sites in the auxiliary chains is taken to be unity.

2.3 The leads

So far, one can compute the S-matrix of any given system; however, it has the restriction of being attached to 1D-chain leads, since it is the only semi-infinite periodic structure handled so far. To generalize the leads, one needs a way to compute the S-matrix of semi-infinite periodic structures.

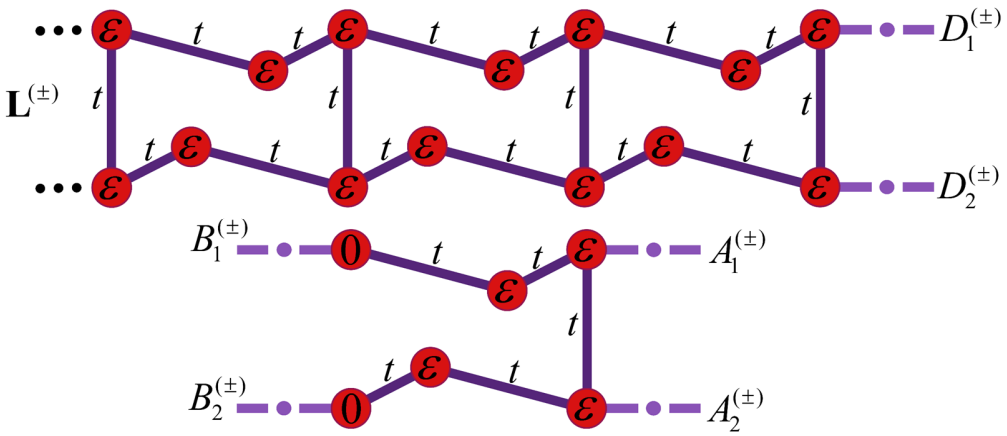

Figure 2.3.- Example of a semi-infinite periodic lead, infinite to the left and finite to the right, and its unitary cell.

Consider a semi-infinite periodic structure, which extends to infinity on the left side, and its unit cell, for example, the ones shown in Fig. 2.3. The S-matrix of the unit cell, $\mathbf{S}^U$, can be written so that it satisfies that

$$\begin{pmatrix} \mathbf{A}^{(-)} \\ \mathbf{B}^{(-)} \end{pmatrix} = \overbrace{\begin{pmatrix} \mathbf{S}_{11} & \mathbf{S}_{12} \\ \mathbf{S}_{21} & \mathbf{S}_{22} \end{pmatrix}}^{\mathbf{S}^U} \begin{pmatrix} \mathbf{A}^{(+)} \\ \mathbf{B}^{(+)} \end{pmatrix}, \tag{2.7}$$

where the system has $2Q$ auxiliary chains attached to it (Q on the left and Q on the right), and $\mathbf{A}^{(\pm)}$ ($\mathbf{B}^{(\pm)}$) is a column vector of Q rows whose entries correspond to the wave amplitudes in the chains on the right (left) of the unit cell.

Now, by using Bloch's theorem, one can obtain a generalized eigenvalue equation

$$\begin{pmatrix} -\mathbf{S}_{11} & \mathbf{I} \\ -\mathbf{S}_{21} & \mathbf{0} \end{pmatrix} \begin{pmatrix} \mathbf{A}^{(+)} \\ \mathbf{A}^{(-)} \end{pmatrix} = \lambda \begin{pmatrix} \mathbf{0} & \mathbf{S}_{12} \\ -\mathbf{I} & \mathbf{S}_{22} \end{pmatrix} \begin{pmatrix} \mathbf{A}^{(+)} \\ \mathbf{A}^{(-)} \end{pmatrix}, \tag{2.8}$$

whose eigenvalues $|\lambda|=1$ can be split into three categories, $|\lambda|<1$, $|\lambda|<1$, and $|\lambda|>1$, which correspond to left- or right-propagating waves, left-evanescent states, and right-evanescent states [20]. Since $\mathbf{A}^{(\pm)}$ have dimension Q, there are a total of $2Q$ eigenvalues λ that can be grouped in Q pairs that satisfy $\lambda\lambda'=1$, which implies that only Q of them are independent, so each left-propagating wave (left-evanescent state) has an associated right-propagating wave (right-evanescent state). Additionally, right-evanescent states are discarded due to not being physically possible in this system. So, considering the $\tilde{Q}$ Bloch-eigenvalues associated to right-propagating waves as part of the independent subset of eigenvalues, we can write such subset as

$$\lambda_j = \begin{cases} e^{i\kappa_j a} & \text{if } j=1,2,\ldots,\tilde{Q} \\ e^{\kappa_j a} & \text{if } j=\tilde{Q}+1,\ldots,Q \end{cases}, \tag{2.9}$$

with corresponding eigenvectors

$$\begin{pmatrix} \mathbf{V}_j^{(+)} \\ \mathbf{V}_j^{(-)} \end{pmatrix}, \tag{2.10}$$

where $\mathbf{V}_j^{(\pm)}$ are column vectors of Q rows.

Using these eigenvectors, one can compute the matrix [20]

$$\mathbf{P} = \begin{pmatrix} \tilde{\mathbf{M}}_2^{(-)}\left[\tilde{\mathbf{M}}_2^{(+)}\right]^{-1} & \mathbf{M}_1^{(-)} - \tilde{\mathbf{M}}_2^{(-)}\left[\tilde{\mathbf{M}}_2^{(+)}\right]^{-1}\tilde{\mathbf{M}}_1^{(+)} \\ \left[\tilde{\mathbf{M}}_2^{(+)}\right]^{-1} & -\left[\tilde{\mathbf{M}}_2^{(+)}\right]^{-1}\mathbf{M}_1^{(+)} \end{pmatrix}, \tag{2.11}$$

where

$$
\begin{aligned}
\mathbf{M}_1^{(\pm)} &= \begin{pmatrix} \mathbf{V}_1^{(\pm)} & \mathbf{V}_2^{(\pm)} & \cdots & \mathbf{V}_{\tilde{Q}}^{(\pm)} \end{pmatrix}, \\
\mathbf{M}_2^{(\pm)} &= \begin{pmatrix} \mathbf{V}_1^{(\mp)} & \mathbf{V}_2^{(\mp)} & \cdots & \mathbf{V}_{\tilde{Q}}^{(\mp)} \end{pmatrix}^*, \\
\mathbf{M}_3^{(\pm)} &= \begin{pmatrix} \mathbf{V}_{\tilde{Q}+1}^{(\pm)} & \mathbf{V}_{\tilde{Q}+2}^{(\pm)} & \cdots & \mathbf{V}_{Q}^{(\pm)} \end{pmatrix}, \\
\tilde{\mathbf{M}}_2^{(\pm)} &\equiv \mathbf{M}_2^{(\pm)} \mathbf{M}_3^{(\pm)}.
\end{aligned}
\tag{2.12}
$$

The S-matrix of the lead, $\mathbf{S}^L$, corresponds to the first $Q+\tilde{Q}$ rows of matrix $\mathbf{P}$, and satisfies

$$
\begin{pmatrix} \mathbf{D}^{(-)} \\ \mathbf{L}^{(-)} \end{pmatrix} = \overbrace{\begin{pmatrix} \mathbf{S}_{11}^L & \mathbf{S}_{12}^L \\ \mathbf{S}_{21}^L & \mathbf{S}_{22}^L \end{pmatrix}}^{\mathbf{S}^L} \begin{pmatrix} \mathbf{D}^{(+)} \\ \mathbf{L}^{(+)} \end{pmatrix}, \tag{2.13}
$$

where $\mathbf{D}^{(\pm)}$ ($\mathbf{L}^{(\pm)}$) is a column vector of Q ($\tilde{Q}$) rows corresponding to the amplitudes of waves on the finite (infinite) side of the lead. Notice that the block $\mathbf{S}_{11}^L$ corresponds to the scattering of waves from the Q auxiliary chains attached to the lead into themselves.

Finally, to obtain a system that consists of a scattering region attached to general semi-infinite leads, one computes the S-matrices of the left and right leads, which have Q_L and Q_R auxiliary chains attached to their finite side respectively, and the S-matrix of the scatterer, who must have a total of Q_L+Q_R auxiliary chains attached to it. Then, one glues Q_L (Q_R) of the scatterer's auxiliary chains to the left (right) lead, resulting in the desired system.

Consequently, we have a method that allows us to compute the S-matrix of any tight-binding system attached to arbitrary semi-infinite periodic leads. It is worth mentioning that this method can be extended to compute the S-matrices as order-N Taylor series, which leads to an exact order-N Taylor series for the conductance [21].

3. Algorithm optimization

When performing numerical calculations, their computational efficiency is of great interest. The more efficient an algorithm is, the less time it takes to compute complex systems compared to others. Therefore, these algorithms can be categorized in function of how their computational time scales with the size of the system.

For example, consider a usual square lattice of $L \times L$ sites. Solving this system with direct diagonalization has a scaling of $O(L^6)$ since one must invert an $L^2 \times L^2$ matrix. Solving it using the transfer matrix method, a circular slicing algorithm [17] or an adaptive slicing algorithm [22] has a scaling of $O(L^4)$. And solving it using methods suitable for sparse matrices [18], since in tight-binding systems most of the entries of the Hamiltonian matrix are zero, has a scaling of $O(L^3)$ if $L \sim 10^3$.

In the following, I propose an algorithm to implement the RSMM and determine its computational complexity as a function of the size of the system. It is worth mentioning that the results of this chapter were also published in Ref. [23].

3.1 Divide-and-Conquer algorithm

As stated in the previous chapter, the RSMM allows us to compute the S-matrix of any tight-binding system by gluing together the subsystems that conform it. Just like a puzzle, where one chooses the total number of pieces, their shape, their size, and their order of placement.

Now, as it can be seen in Eq. (2.3), when gluing two systems together, one must compute the inverse of an $N \times N$ matrix, where N is the number of sites of each system that are being fused together. This operation has a computational complexity of $O(N^3)$. Therefore, an optimal implementation of the RSMM has to glue together systems that have the smallest N possible and do so in the least number of steps.

To achieve this, in the general case, consider the algorithm shown in Fig. 3.1. One starts with an arbitrary scattering region and proceeds to split it in two subsystems, preferably in half. Then, one takes each of these two subsystems and

split each in another two subsystems. One repeats this process iteratively, keeping track of the divisions that are made, until the subsystems consist of only a single site. Finally, one computes the S-matrices of this single site structures and starts gluing them together following the reverse order.

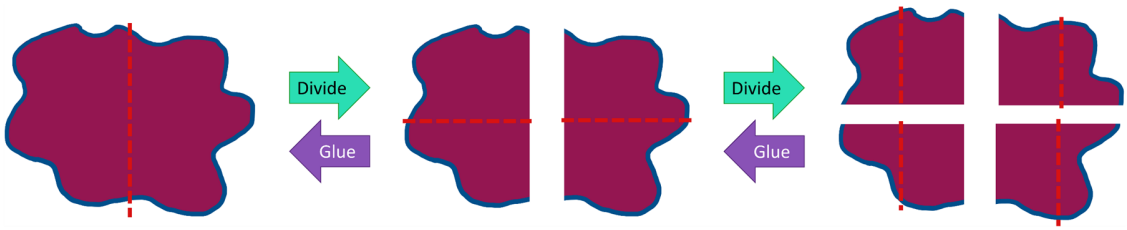

Figure 3.1.- Diagram of the operation of the Divide-and-Conquer algorithm. The system is divided recursively in halves until reaching one-site systems, then, the S-matrices are computed by gluing them together in the inverse order.

Notice that dividing a system in two is quite arbitrary, and the optimal way to do so strongly depends on the geometry of the system and the coordination number of its sites. This is because we seek to divide the system as evenly as possible to distribute the computational load of generating each subsystem as much as we can, and the higher the coordination number of the sites, the more connections we must make.

However, if we restrict our systems to crystal systems and slightly disordered periodic systems, for example, systems arranged in a Bravais lattice with bonds only between nearest neighbors, a Honeycomb lattice, a Bravais lattice with small dislocation and sheer impurities, etc. Then we can do the divisions by taking the sites physical coordinates and splitting the system in half along its widest dimension. The system's periodic structure guarantees that such division will produce two somewhat even subsystems and that the number of auxiliary chains to be fused together in each gluing step depends only on the number of frontier sites.

It is worth mentioning that this criteria for the division of a system can also be applied to systems that have their sites randomly distributed within a finite region of space as long as they are uniformly distributed. In this case, one also has to bear in mind that the computational time required to compute these systems is dependent on the length of the bonds. This is because a bond between two sites that are far

from each other translates into one extra dimension for the S-matrices of the subsystems that will take several gluing steps to disappear since, with this algorithm, the further two sites are, the more steps are required to glue them into the same subsystem.

Now, in order to obtain an estimation of the computational complexity of this algorithm consider a scatterer that consists of L^2 sites distributed in a square lattice of $L \times L$ sites with connections only between nearest neighbors, where the on-site energies and the hopping parameters are completely arbitrary. Since the division process will end up with subsystems that consist of a single site, let us define the time required to compute the S-matrix of a single site as τ_0. This implies that this system requires a time $L^2\tau_0$ to compute the S-matrices of the individual sites.

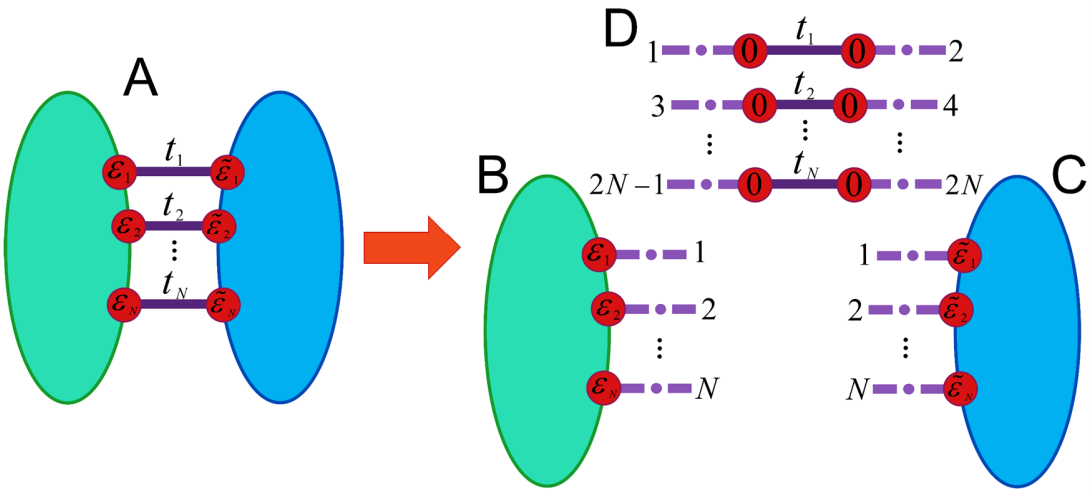

Figure 3.2.- Example of how the division and gluing process is performed. When splitting a system in two, the bonds that were attaching them together become an independent third system that is responsible for gluing them back together. Only the first N auxiliary chains of B and C are shown, but they can have more of them. The odd-numbered chains of D are glued to the auxiliary chains on B, whereas the even-numbered chains of D are glued to the auxiliary chains of C.

To consider the time required by all the gluing steps, first we need to take a closer look at exactly how the division and gluing are performed. As it can be seen in Fig. 3.2, when splitting a system, A, into subsystems B and C, one identifies the N bonds that are attaching B and C together, then one separates B and C by replacing those bonds with auxiliary chains, and considers the removed bonds as a

new system, D. System D becomes an auxiliary system that is essential to glue systems B and C together since it contains the information of the hopping parameters between these two.

The S-matrix of system D, $\mathbf{S}^{\mathrm{D}}$, can be easily computed following the expression for the S-matrix of a bond structure shown in Eq. (2.4). Therefore, if $\mathbf{S}_i$ is the S-matrix of bond i, then $\mathbf{S}^{\mathrm{D}}$ is given by

$$\mathbf{S}^{\mathrm{D}} = \begin{pmatrix} \mathbf{S}_1 & \mathbf{0} & \cdots & \mathbf{0} \\ \mathbf{0} & \mathbf{S}_2 & \ddots & \vdots \\ \vdots & \ddots & \ddots & \mathbf{0} \\ \mathbf{0} & \cdots & \mathbf{0} & \mathbf{S}_N \end{pmatrix}, \tag{3.1}$$

where $\mathbf{0}$ is the 2×2 null matrix. Additionally, this same logic leads us to consider systems B and C together as a system $\tilde{\mathrm{B}}$, whose S-matrix is given by

$$\mathbf{S}^{\tilde{\mathrm{B}}} = \begin{pmatrix} \mathbf{S}^{\mathrm{B}} & \mathbf{0} \\ \mathbf{0} & \mathbf{S}^{\mathrm{C}} \end{pmatrix}, \tag{3.2}$$

notice that the off-diagonal matrices are null since systems B and C are decoupled. Consequently, to glue B and C together, one applies the RSMM, *i.e.,* Eq. (2.3), to $\mathbf{S}^{\mathrm{D}}$ and $\mathbf{S}^{\tilde{\mathrm{B}}}$. Notice that the rows and columns of $\mathbf{S}^{\mathrm{D}}$ and $\mathbf{S}^{\tilde{\mathrm{B}}}$ must be permuted so that they satisfy the decomposition defined in Eq. (2.2)

Returning to the computational time estimation, we have that when gluing two systems with N bonds, the time required to generate $\mathbf{S}^{\mathrm{D}}$ is $N\tau_1$, where τ_1 is the time required to compute the S-matrix of a single bond, and the time to glue systems D and $\tilde{\mathrm{B}}$ together is aN^3, because this time is dominated by the inversion of a $2N\times 2N$ matrix whose computational complexity is $O(8N^3)$ and the factor a absorbs the effect of the factor 8.

Now, for approximation purposes and since the interest of the scaling is for large values of L, consider that there exists an integer q such that $1 \ll L \approx 2^q$. Therefore, the total computational time is

$$\begin{aligned}\mathrm{time}(L) \approx \tau_0 L^2 \quad & + \sum_{j=0}^{q-1}\left[\tau_1\left(2^{2j}\right)\left(\frac{2L}{2^j}\right) + a\left(2^{2j}\right)\left(\frac{L}{2^j}\right)^3\right] \\ & + \sum_{j=1}^{q}\left[\tau_1\left(2^{2j-1}\right)\left(\frac{2L}{2^j}\right) + a\left(2^{2j-1}\right)\left(\frac{L}{2^j}\right)^3\right],\end{aligned} \tag{3.3}$$

where the first (second) sum accounts for the time of computing the bonds matrices and the gluing processes for the vertical (horizontal) divisions, assuming the first division was done vertically. After solving the sums, we get

$$\begin{aligned}\mathrm{time}(L) \quad & \approx \tau_0 L^2 + \sum_{j=0}^{q-1}\left[\tau_1\left(2^{j+1}L\right) + a\left(\frac{L^3}{2^j}\right)\right] + \sum_{j=1}^{q}\left[\tau_1\left(2^{j}L\right) + a\left(\frac{L^3}{2^{j+1}}\right)\right] \\ & = \tau_0 L^2 + 2\tau_1 L\frac{1-2^q}{1-2} + aL^3\frac{1-(1/2)^q}{1-(1/2)} + \tau_1 L\left(\frac{1-2^{q+1}}{1-2}-1\right) + \frac{aL^3}{2}\left(\frac{1-(1/2)^{q+1}}{1-(1/2)}-1\right) \\ & = \tau_0 L^2 + 2\tau_1 L\left(2^q-1\right) + 2aL^3\left(1-(1/2)^q\right) + \tau_1 L\left(2^{q+1}-2\right) + \frac{aL^3}{2}\left(1-(1/2)^q\right) \\ & = \tau_0 L^2 + 4\tau_1 L\left(2^q-1\right) + \frac{5aL^3}{2}\left(1-(1/2)^q\right) \\ & \approx \tau_0 L^2 + 4\tau_1 L\overbrace{(L-1)}^{\approx L} + \frac{5aL^3}{2}\left(1-L^{-1}\right) \\ & \approx \left(\tau_0 + 4\tau_1 - \frac{5a}{2}\right)L^2 + \frac{5a}{2}L^3.\end{aligned} \tag{3.4}$$

So, the total time required to compute the S-matrix of a square lattice of $L\times L$ sites using the Divide-and-Conquer algorithm is approximately given by

$$\mathrm{time}(L) = b_1 L^2 + b_2 L^3, \tag{3.5}$$

where b_1 and b_2 are fixed scalars.

Now, it is preferable that Eq. (3.5) has the form $\mathrm{time}(L) = c_1 L^{c_2}$ so that the computational complexity of the algorithm would simply be $O(L^{c_2})$. To determine c_2 one can take the derivative of $\log\left[\mathrm{time}(L)\right]$ with respect to $\log\left[L\right]$, on the one hand one gets

$$\frac{\mathrm{d}}{\mathrm{d}\log\left[L\right]}\left\{\log\left[\mathrm{time}(L)\right]\right\} = \frac{\mathrm{d}}{\mathrm{d}\log\left[L\right]}\left\{\log\left[c_1\right] + c_2\log\left[L\right]\right\} = c_2, \tag{3.6}$$

and on the other hand,

$$\frac{\mathrm{d}}{\mathrm{d}\log\left[L\right]}\left\{\log\left[\mathrm{time}(L)\right]\right\} = \frac{\mathrm{d}}{\mathrm{d}\log\left[L\right]}\left\{\log\left[b_1 L^2 + b_2 L^3\right]\right\} = \frac{2b_1 L^2 + 3b_2 L^3}{b_1 L^2 + b_2 L^3}, \tag{3.7}$$

where I used that

$$\frac{\mathrm{d}\, L^{\alpha}}{\mathrm{d}\log\left[L\right]} = \alpha L^{\alpha-1} \frac{1}{\frac{\mathrm{d}}{\mathrm{d}\, L}\left\{\log\left[L\right]\right\}} = \alpha L^{\alpha} \tag{3.8}$$

for $\alpha \neq 0$. After simplifying Eq. (3.7) and equating it to Eq. (3.6), one gets

$$c_2 = 2 + \frac{1}{1 + \frac{b_1}{b_2}\frac{1}{L}}. \tag{3.9}$$

Equation (3.9) is a local scaling approximation and implies that for small values of L, the computational complexity of the Divide-and-Conquer algorithm is $O(L^2)$, whereas for large L it is $O(L^3)$, and the scaling undergoes a soft transition between these two limit behaviors.

In the following section, I analyze the computational performance of this algorithm for various scattering regions attached to semi-infinite periodic chains as leads.

3.2 Computational performance

Figure 3.3 shows with red squares the computational time required to determine the S-matrix, using the Divide-and-Conquer algorithm, of a square lattice of $L \times L$ sites as a function of L. These values fit the curve $b_1 L^2 + b_2 L^3$ (red line) with $b_1 = 8.122 \times 10^{-5}$ and $b_2 = 3.034 \times 10^{-8}$, which, after substituting in Eq. (3.9), tell us that for $L \sim 10^3$ the scaling goes as $L^{2.27}$, representing an improvement in the performance of transport calculations. Even more, if $L \leq 2676$ one gets $c_2 \leq 2.5$; which means that for approximately seven million total sites, this algorithm maintains a scaling under the L^3 mark of other state-of-the-art methods.

For comparison, Fig. 3.3 also shows with blue circles the computational time needed to compute the transfer matrix of the same square lattices. The formula used to determine such matrices and its deduction is presented in Appendix A. Points for

large L are fitted by $\alpha L^{3.971}$ (blue line), with $\alpha = 1.517 \times 10^{-9}$. Given the small value of α, the transfer matrix method is faster than the Divide-and-Conquer algorithm for $L \leq 250$; however, the difference in times for the same system in this region is less than an order of magnitude. Moreover, for large systems, the Divide-and-Conquer algorithm presents times smaller than the ones of the transfer matrix by an order of magnitude and without needing to realize cumbersome calculations as the ones shown in Appendix A.

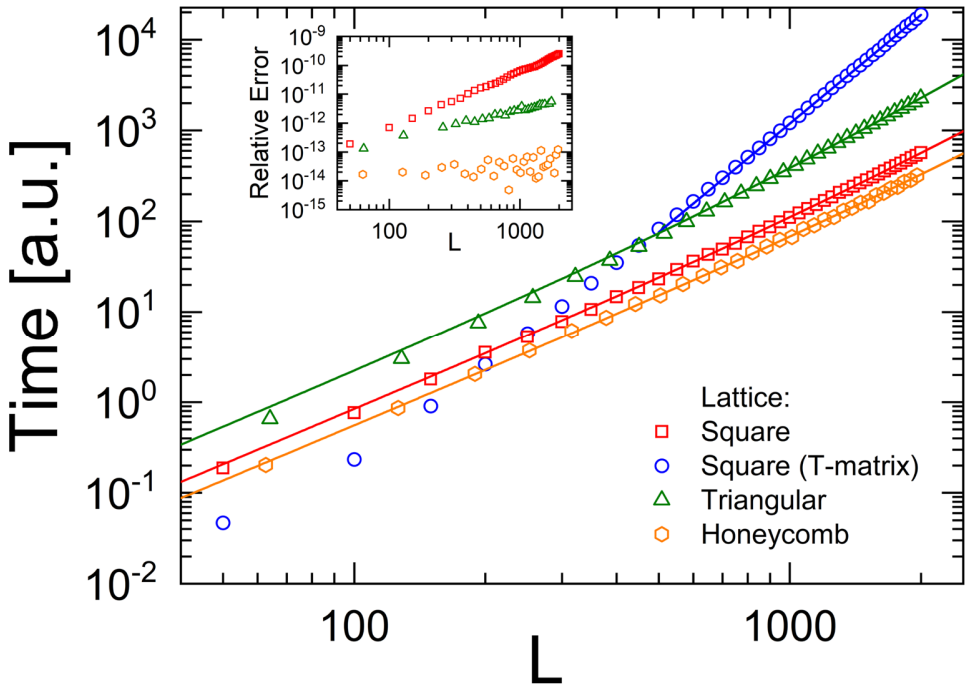

Figure 3.3.- Computational time to determine the S-matrix of square (red squares), triangular (green triangles) and honeycomb (orange hexagons) lattices using the divide-and-conquer algorithm, and to determine the transfer matrix, T-matrix, of a square lattice (blue circles). The number of sites in each system is $N = L^2$ and they are within a square area. Lines correspond to fittings as detailed in the text. (Inset) Relative error on the S-matrix for each lattice using the divide-and-conquer method.

To analyze the behavior of the Divide-and-Conquer algorithm in other lattices, Fig. 3.3 further shows the computational times to compute the S-matrices, using this algorithm, of squared areas of triangular (green triangles) and honeycomb (orange hexagons) lattices. In these systems, $L = \sqrt{N}$, where N is the total number of sites.

For the triangular lattice, the computational times fit the curve $b_1 L^2 + b_2 L^3$ (green line) with $b_1 = 2.054 \times 10^{-4}$ and $b_2 = 1.830 \times 10^{-7}$; whereas for the honeycomb lattice they fit the same curve (orange line) but with $b_1 = 5.412 \times 10^{-5}$ and $b_2 = 1.415 \times 10^{-8}$. The fact that the coefficients b_1 and b_2 are smaller for the honeycomb lattice than for the triangular lattice is a consequence of the aforementioned dependance of the algorithm on the coordination number of the lattice's sites.

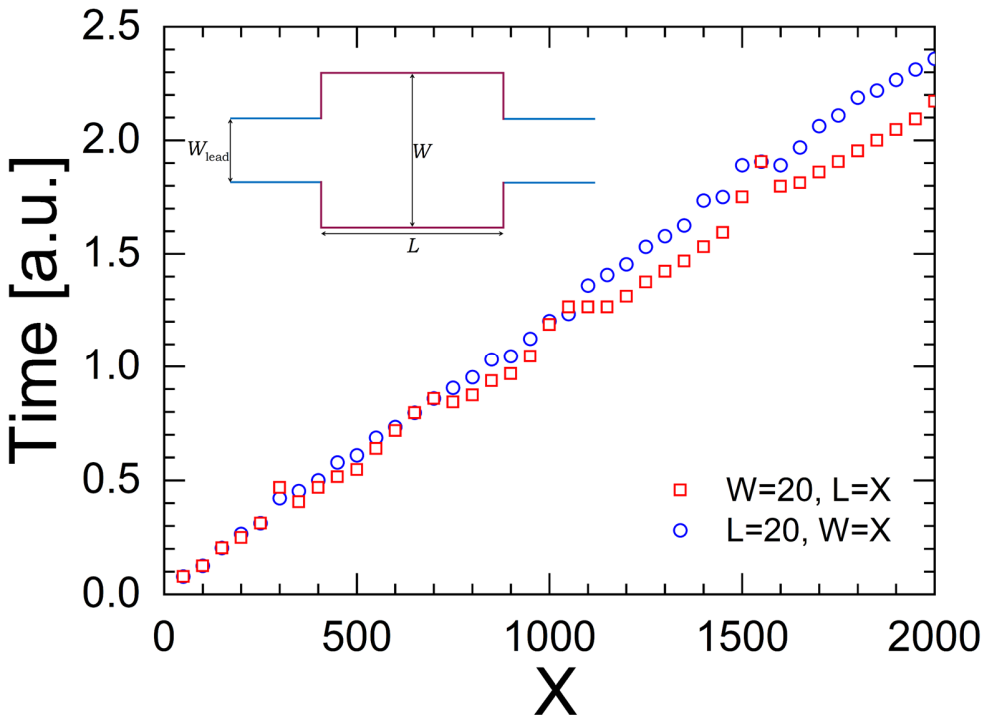

Figure 3.4.- Computational time to determine the S-matrix of a square lattice of fixed width, $W = 20$ sites, and varying L (red squares), and one of fixed length, $L = 20$ sites, and varying W (blue circles) using the divide-and-conquer algorithm. In both cases $W_{\text{lead}} = 20$ chains.

Additionally, given that the probability flux conservation, $T + R = 1$, must be satisfied for every wave that enters the scattering region, the inset in Fig. 3.3 shows the average of $|T + R - 1|$ as an estimation of the relative error in the numerical calculation of the S-matrix. This leads to the conclusion that the Divide-and-Conquer

algorithm is numerically stable, with precision better than the ninth significative figure even for $L \sim 10^3$.

Finally, consider the cases of scattering regions with high aspect ratios. If the system consists of a square lattice of $L \times W$ sites, as shown in the inset of Fig. 3.4, where $W \ll L$, the Divide-and-Conquer algorithm leads to the computation of L/W S-matrices of blocks of $W \times W$ sites. Then, the scaling of the computational times goes as $b_1 LW + b_2 LW^2$. Consequently, for fixed W, the Divide-and-Conquer algorithm is linear in L, which is on par with other recursive methods [17,22,24]. On the other hand, if $L \ll W$ then the computational time goes as $b_1 LW + b_2 L^2 W$, which is linear in W. Figure 3.4 presents the computational time for these two types of square lattices, red squares for $W \ll L$ and blue circles for $L \ll W$. Notice that the scaling behavior is indeed linear on the largest dimension regardless of the orientation of the scattering region.

In summary, the implementation of the RSMM following the Divide-and-Conquer algorithm can be done on any system but has its peak performance on crystal systems and slightly disordered periodic systems, which stays under the L^3 scaling mark of other state-of-the-art recursive methods. Additionally, in systems with high aspect ratios, its scaling is linear in the largest dimension, which is on par with other methods.

4. Conductance in random networks

The Landauer conductance is usually computed for crystal systems or slightly deformed versions of them. Even when the effects of disorder are analyzed, they are only introduced as randomized values of the on-site energies and/or the hopping parameters. Therefore, in this chapter, the effect of randomizing the presence of a connection between sites on the conductance of a system is explored. In other words, the Landauer conductance is analyzed in three of the most common random networks: the Erdös-Rényi network, the Small World network, and the Scale Free network. The Small World network has been previously studied under a continuous-time quantum walk approach [25] and also via the Green Function method for a construction rule different to the one handled in this work [26]. The Scale Free network has also been studied but from Kirchhoff's classical viewpoint [27].

The conductance of all three networks is computed using the Divide-and-Conquer algorithm considering their sites to have null on-site energy, for them to be located within an area of $100nm \times 100nm$, and two cases for the types of connections between sites. The first is to consider that any pair of sites that are connected have a fixed hopping parameter t; however, this case, although interesting, is not very consistent with the tight-binding approximation, since two sites that are close to each other can be unlinked and, at the same time, be linked to sites that are far away from them. On the other hand, the second case is to take the connections to be chains of $N+1$ sites, counting the two sites that are being connected, of null on-site energy and hopping parameter $t=1$, where $N = \max\left(\text{int}\left[d/0.2\right],1\right)$ and d is the distance between the pair of sites. This implies that the connections between sites are performed manually by introducing 1D-chains into the system whose sites are $0.2nm$ apart, which is more physically viable than the first case.

This second case could be utilized to broaden the understanding of the behavior of randomly connected single wall carbon nanotubes, whose analysis and elaboration are of interest due to their performance as thin film transistors [28,29].

It is worth mentioning that to improve computational performance when the connections consist of 1D-chains, instead of constructing the chains site by site

using the RSMM, the S-matrix of such chains is computed using the formula obtained in Appendix B.

4.1 Erdös-Rényi

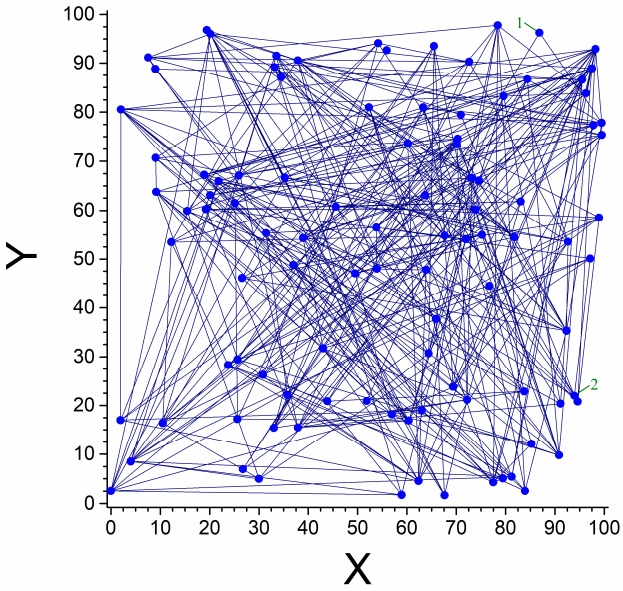

Figure 4.1.- Example of an Erdös-Rényi network. $N = 100$ *nodes where each pair has a probability* $P = 0.07$ *of being connected. The green numbers signal the nodes between which the Landauer conductance was computed.*

This network consists of having a fixed number of nodes, N, and then connecting each possible pair of nodes with probability P. An example of this type of network is shown in Fig. 4.1. Notice that if $P \ll 1$, then it is very unlikely to have connected nodes and the network is essentially disconnected, *i.e.*, there is no path that connects any two given nodes. On the other hand, if $P \approx 1$, then almost every pair of nodes is connected and there exists a minimum number of steps (jumps between connected nodes) to go from one node to any other. The transition between these two behaviors occurs at the transition probability of $P = \log(N)/N$ [30].

Now, the conductance is computed between two randomly selected sites of an Erdös-Rényi network of $N = 100$ total sites, where their positions were chosen randomly with a uniform probability distribution. Following the example shown in Fig. 4.1, the transmission of a particle arriving at the site marked with the number one

and leaving the one marked with a two is analyzed, where each of these sites is attached to an auxiliary chain of null on-site energy and hopping parameter $t_C = 1$. Therefore, the conductance of the system is calculated using the second formula of Landauer, Eq. (1.4), which is proportional to the transmission function, $T(E)$.

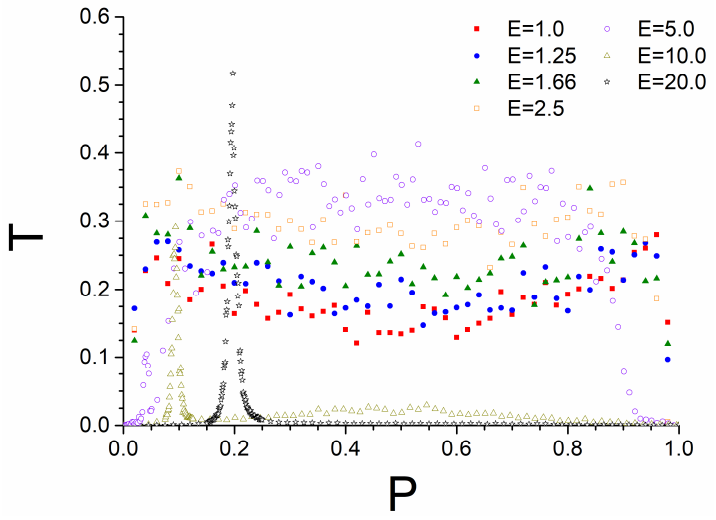

Figure 4.2.- Average transmission function as a function of the reconnection probability, P, of the Erdös-Rényi network for $N = 100$, and various energies, E, when the links consist of bonds of hopping parameter $t = 1$.

Figure 4.2 shows the average transmission function of the network for a particle with energy E as a function of the probability of connecting two sites, and for the case when the links in the network are bonds of hopping parameter $t = 1$. Notice that since the value of t sets the scale of the energy, *i.e.,* we have the dimensionless parameter E/t, then changing the value of E keeping t fixed is equivalent to keeping E fixed and varying t as long as $E \neq 0$. Each data point corresponds to the average of 1000 iterations for fixed P.

Now, to understand these results we consider the energy spectra shown in Fig. 4.3. Figure 4.3(a) shows the colormap of the normalized density of states as a function of the energy and the probability P for the Erdös-Rényi network, whereas Fig. 4.3(b) also shows the colormap of the density of states but for a periodic chain

with connections to the q nearest neighbors and periodic boundary conditions as a function of the energy and q.

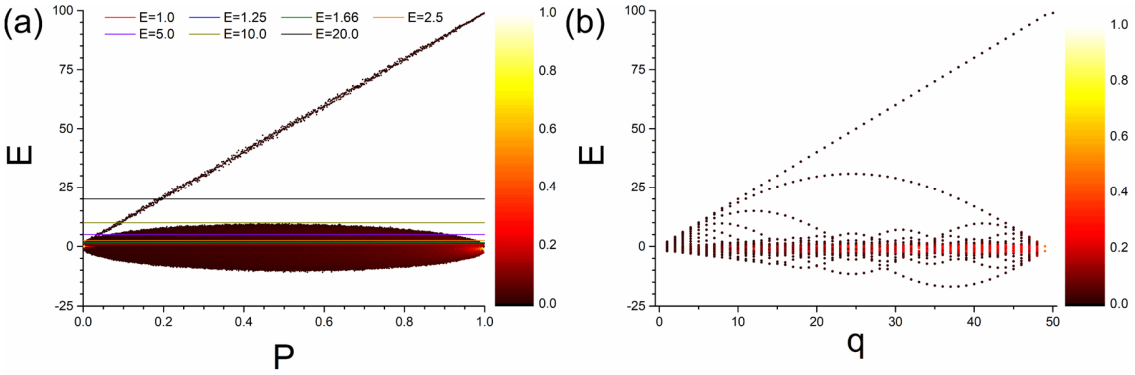

Figure 4.3.- Colormap of the normalized density of states for (a) the Erdös-Rényi network with connections consisting of bonds of hopping parameter $t=1$ as a function of the particle's energy, E, and the probability of connection, P; and (b) a periodic chain with connections to the q nearest neighbors and periodic boundary conditions as a function of E and q.

Notice that both energy spectra are quite similar to each other; moreover, they perfectly agree on the straight line that reaches $E=100$, which for fixed P (q) corresponds to the energy of the base state of the system since we are considering $t=1$. We can infer that the missing curves on Fig. 4.3(a), that are present on Fig. 4.3(b), actually collapsed into the oval due to random effects. Even more, it is well known that the average degree of an Erdös-Rényi network is NP, so we can conclude that this network with this type of connection behaves similarly to a periodic chain connected to the $q=NP/2$ nearest neighbors with periodic boundary conditions.

Furthermore, the energies marked in Fig. 4.3(a) correspond to the ones chosen in Fig. 4.2. Observe that the presence and number of eigenstates of the system for fixed energy and probability is strongly correlated to its transmission function; this explains the abrupt change in the transmission spectrum as E increases. Once the energy is large enough, greater than 10 in this case, we have that the only state that can contribute to the conductance of the system is the base state, that is why the conductance spectrum as a function of the probability suddenly changes into a single peak whose width is related to the randomness of the system.

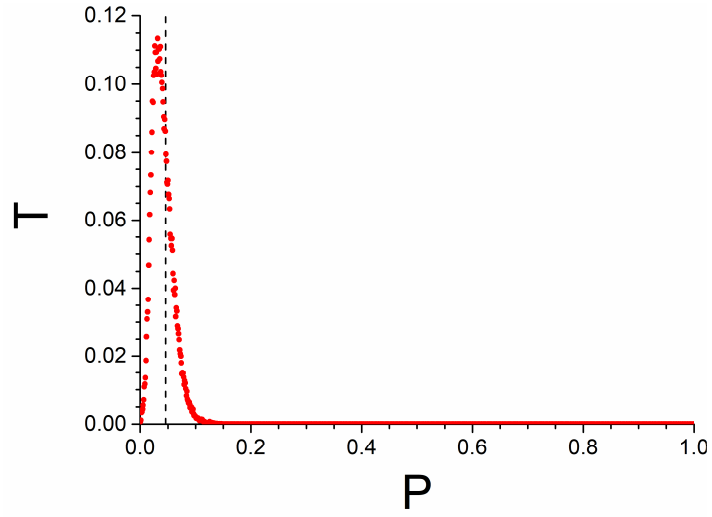

Figure 4.4.- Average transmission function as a function of the reconnection probability, P, of the Erdös-Rényi network for $N = 100$, and $E = 1$, when the links consist of 1D chains (red circles). The transition probability, $\log(N)/N$, is marked with a vertical dashed line.

On the other hand, when the connections consist of 1D-chains, the average transmission function is sharply peaked close to the transition probability of $\log(N)/N$, as shown in Fig. 4.4. To try to explain this, we can think of the state of the network as P increases. First, it is very unlikely for any two sites to be attached so the conductance starts from zero. Then, it starts to become more viable for there to exist a path between a pair of nodes, but there is not a path between any pair of nodes, so the conductance starts increasing without reaching a maximum value. Next, P approaches the transition probability, where there are still few connections in the network, but there exists a path between every pair of chosen sites; this would imply that no two sites would be isolated from each other, and the transmission function should reach a maximum value. However, with more connections there is also more interference in each site, which would start to reduce the conductance of the system; hence, the maximum value is reached a little below the transition probability. Finally, the system starts to be so connected that the destructive interference present in the system increases to the point that after $P \approx 0.15$, the system is an insulator.

4.2 Small World

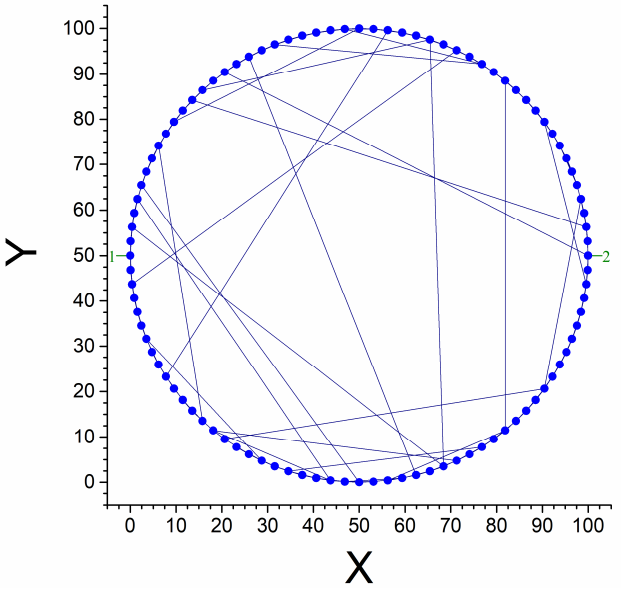

Figure 4.5.- Example of a Small World network of $N = 100$ nodes. Each node is connected to its 2 neighbors clockwise and each link has a probability $P = 0.075$ of being randomly reconnected. The green numbers signal the nodes between which the Landauer conductance was computed.

This network consists of a fixed number of sites, N, uniformly distributed along the perimeter of a circle. They start by being connected to their first q neighbors clockwise, notice that every site starts with a total of $2q$ links. Then, for each site, each of the clockwise links is randomly reconnected to another site with probability P. To be in the Small World regime, the parameters of the system have to satisfy $1 \ll \log(N) \ll 2q \ll N$ and have a probability of reconnection of $0.01 < P < 0.1$, like the example shown in Fig. 4.5. This allows just enough links to be rewired so that the number of steps, *i.e.,* the number of jumps between connected sites, needed to go from one site to any other is greatly reduced compared to the starting condition while keeping the majority of the connections between close sites [31].

Now, the conductance is computed between two diametrically opposite sites, as shown in Fig. 4.5, using the second formula of Landauer for the case of $N = 100$ and $q = 2$. As before, the conductance corresponds to the transmission of a particle

arriving through a semi-infinite periodic chain of null on-site energies and hopping parameter $t_C = 1$ attached to site one and leaving through a similar chain attached to site two.

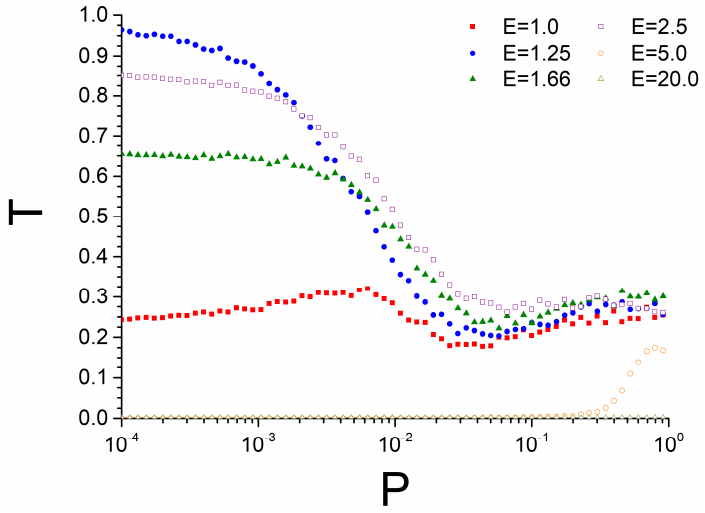

Figure 4.6.- Average transmission function as a function of the reconnection probability, P, of the Small World network for $N = 100$, and various values of E, when the links consist of bonds of hopping parameter $t = 1$.

Figure 4.6 shows the average transmission function of the system as a function of the probability of rewiring a connection when the links consist of bonds of hopping parameter $t = 1$, each data point corresponds to the average of one thousand iterations. As in the Erdös-Rényi network, these results are easier to explain considering the energy spectrum of such Small World network shown in Fig. 4.7. One can notice that for small P the eigen energies of the system are well discretized, then, as the probability of reconnection increases, these energies start to spread out. This spreading can be seen to start as soon as the system is close to entering the Small World regime, and, when P is large enough to leave this regime, it is so strong that there is no sign of the initial energy levels.

Now, the horizontal dashed lines in Fig. 4.7 correspond to the energies chosen in Fig. 4.6, the energy $E = 20$ is not considered since it is so far away from the eigen energies that it will trivially have a zero transmission. Note that for small probabilities the transmission of the system is greater if the energy for which it is being evaluated

is closer to an eigen energy and it quickly decreases if the energy is far from them. Also, inside the Small World regime, one can see a considerable change in the conductance of the system as if it started to forget the energy levels; this is due to the eigen energies starting to spread out. Finally, when leaving the Small World regime, the eigen energies are so spread out that the transmission function is essentially the same for all the energies that are inside the bandwidth. Additionally, the fact that the maximum allowed energy, which once again corresponds to the base state of the system since $t = 1$, increases after leaving the Small World regime explains why the system's conductance is no longer zero for $E = 5$.

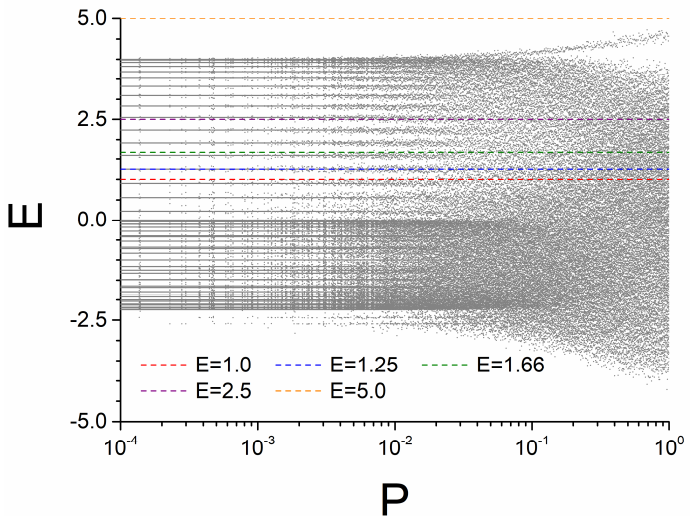

Figure 4.7.- Energy spectrum (gray dots) of a Small World network with $N = 100$ sites as a function of the reconnection probability, P, when the links consist of bonds of hopping parameter $t = 1$.

These results suggest that the conductance of the system is very susceptible to reconnections while in the Small World regime, but it becomes independent of them when leaving it. It also becomes independent of the particle's energy as long as it is inside the eigen energy bandwidth. Also, for P closer to 1 the network converges to an Erdös-Rényi network, which in this case can be corroborated by noticing that the conductance of this system for these probabilities is consistent with the transmission of the Erdös-Rényi network for $P = 0.04$, since it is when both networks have an average degree of 4.

On the other hand, the average transmission function for a particle with energy $E=1$ as a function of the probability of rewiring a link, P, when the links consist of 1D-chains is shown in Fig. 4.8, each data point corresponds to one thousand iterations. Notice that the spectra is almost identical to the one corresponding to the case where the links were bonds of hopping parameter $t=1$. The main difference is after leaving the Small World regime, *i.e.,* for $P>0.1$; here we have that instead of converging to the Erdös-Rényi spectrum, the transmission collapses to zero due to destructive interference effects that the 1D-chains introduce to the system.

Therefore, we can conclude that the system's conductance is independent of the type of links up until leaving the Small World regime, where it will either remain fairly constant or it will become zero depending on the type of link.

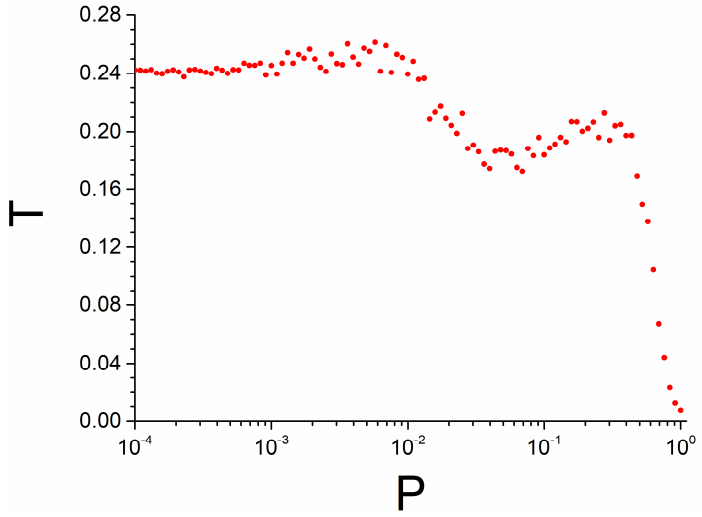

Figure 4.8.- Average transmission function as a function of the reconnection probability, P, of the Small World network for $N=100$ when the links consist of 1D chains.

4.3 Scale Free

The simplest way to construct this network is to start with n_0 fixed sites that are arbitrarily connected between them, *i.e.*, site i is connected to k_i sites, where $k_i=1,2,\ldots,n_0-1$, and k_i is known as *the degree of site* i. Then, one adds another site to the system and connects it to m sites, where m is a fixed value that satisfies

that $1 \le m \le n_0$, and the probability of connecting this new site to the pre-existing site i is given by

$$p_i = \frac{k_i}{\sum_j k_j}, \tag{4.1}$$

with the sum in the denominator running over all the pre-existing sites. The expression in Eq. (4.1) is known as a preferential attachment condition, since a new site is more likely to attach to a site that already has many connections. One continues to add sites to the system following this procedure until the desired total number of sites, N, is reached. This results in the probability distribution of the degree of the nodes taking the form

$$P(k_i) \sim k_i^{-3}, \tag{4.2}$$

which is a power law distribution, hence the name of Scale Free [32]. An example of this network is shown in Fig. 4.9, where the size of the sites is proportional to their degree, so it is easier to see the sites with high degree, also known as *hubs*.

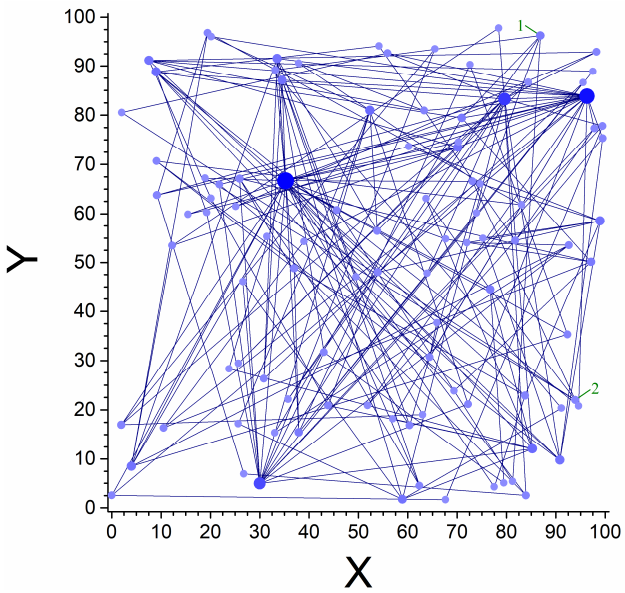

Figure 4.9.- Example of a Scale Free network of $N = 100$ nodes with degree distribution $P(k_i) \sim k_i^{-3}$. The size of the sites is just to help visualize the hubs.

Now, in contrast to the previous networks, the conductance is computed between two randomly selected nodes from the initial n_0 ones for the case with $n_0 = 3$ and $m = 2$. Since it is the conductance between two nodes inside the system, the appropriate formula is Landauer's first formula, Eq. (1.5). This change of focus is also driven by the fact that the conductance of a Scale Free network was analyzed in Ref. [27] from a classical viewpoint, which is more compatible with Landauer's first formula.

Figure 4.10 shows with dashed lines the cumulative distribution function (CDF) of this conductance, where $G_0 = e^2 / h$ was defined, for various combinations of the particle's energy, E, the total number of sites, N, and the type of connections, bonds or 1D-chains. It also shows with a solid line the fit of the power law $\alpha x^{-0.975}$ to each of these CDFs. The independence of such fit with respect to N was to be expected due to the scale free property of this network.

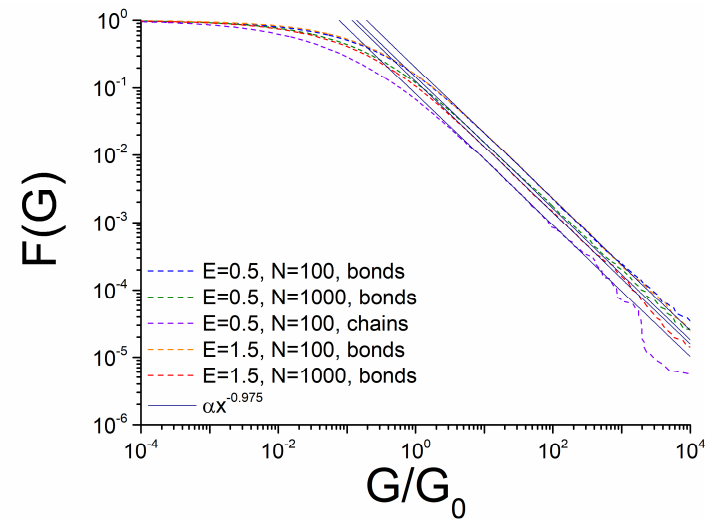

Figure 4.10.- Cumulative distribution function for the conductance, G, of a Scale Free network for various energies, number of nodes, and both types of connections (dashed lines). All solid lines are the same power law fit for each distribution.

Notice that this result implies that the conductance of the system for fixed E, N, and type of connection is not well characterized by its average over a large number of iterations, unlike the past networks. Additionally, the power law seen in

Fig. 4.10 is predicted to have an exponent of -4 from the classical point of view [27], which greatly differs from the exponent of -0.975 obtained with quantum considerations. This implies that, regardless of the size of the system or the type of connection in it, quantum effects make the CDF of the conductance have a thicker tail.

Conclusions

In this work, an improvement in the computational performance of recursive methods for the calculation of the Landauer conductance of quantum nanojunctions under the tight-binding approximation is proposed. Such enhancement is based on the implementation of the Recursive Scattering Matrix Method following a Divide-and-Conquer algorithm, which consists of iteratively dividing the desired system into halves and computing its S-matrix by gluing it back in reverse order. This new algorithm leads to

1) A computational complexity with a scaling that stays under the L^3 mark of other state-of-the-art recursive methods for systems of size $L \times L$.
2) A computational complexity with a linear scaling on the largest dimension of systems with high aspect ratios, which is on par with other recursive methods.
3) An order of magnitude improvement in computational time compared to the transfer matrix method for systems of approximate size $10^3 \times 10^3$ sites.
4) A more visual handling of the system under study due to the use of the physical coordinates of the sites.

This method was implemented for the study of the conductance in randomly connected nanostructures. Essentially, the systems studied followed the construction rules of three of the most common random networks, and two types of links were studied. The main characteristics found in each of them were

1) Erdös-Rényi network: If the links consist of bonds, then the average conductance as a function of the link probability is quite uniform for small energies, and it shows a sharp peak for large energies where only the base state of the system can contribute to the transmission. If the links consist of 1D-chains, then the conductance spectrum consists of only one sharp peak close to the transition probability between disconnected and connected network.
2) Small World Network: If the links are bonds, then, for small probabilities, the conductance strongly depends on how close the particle's energy to the eigen energies of the system is; and, as the probability of reconnection increases, the system forgets these energy levels and converges to an Erdös-Rényi

network, where the strongest change in the conductance happens inside the Small World regime. If the links are 1D-chains, then the system's conductance only differs from the previous case when the probability of reconnecting a link is greater than 0.1. This is due to interference effects that end up collapsing the conductance to zero.

3) Scale Free Network: The cumulative distribution function of the conductance of this system follows a power law of $x^{-0.975}$, which is independent of the energy of the particle, the number of sites, and the type of links. Classically, this exponent is expected to be -4, so quantum effects thicken the tail of the distribution.

In summary, the Divide-and-Conquer algorithm presents a better performance for real sized systems compared to other state-of-the-art recursive methods, so it would be quite useful to calculate physical properties of such systems under the tight-binding approximation. Also, future works could translate this algorithm to the Recursive Green Function methods, since some of them have a modular implementation. Additionally, the performance of this algorithm could be increased via a parallel implementation since the computation of the subsystems can be split into different processors. The algorithm could also be optimized for general systems if their division into subsystems is made with a more general criteria than the one handled in this work; for example, using a cluster finding algorithm to find the most even division of the system. Finally, the analysis presented for the conductance in random networks could be useful to describe the behavior of systems that consist of many randomly connected nanowires, which can be used to make wearable triboelectric nanogenerators [33], or maybe even amorphous systems. It could also serve to study lattices with non-local network couplings [34], although more analysis of random networks, presented or not in this work, is still required to obtain a more detailed understanding of the behavior of physical quantities in random systems.

References

[1] Landauer R 1957 Spatial Variation of Currents and Fields Due to Localized Scatterers in Metallic Conduction *IBM J. Res. Dev.* **1** 223–31

[2] Landauer R 1970 Electrical resistance of disordered one-dimensional lattices *Philos. Mag.* **21** 863–7

[3] Ryndyk D 2016 *Theory of Quantum Transport at Nanoscale* vol 184 (Cham: Springer International Publishing)

[4] Datta S 1995 *Electronic Transport in Mesoscopic Systems* (Cambridge University Press)

[5] Bagwell P F and Orlando T P 1989 Landauer's conductance formula and its generalization to finite voltages *Phys. Rev. B* **40** 1456–64

[6] Khondker A N and Alam M A 1991 Büttiker-Landauer conductance formulas in the presence of inelastic scattering *Phys. Rev. B* **44** 5444–52

[7] Maslov D L and Stone M 1995 Landauer conductance of Luttinger liquids with leads *Phys. Rev. B* **52** R5539–42

[8] Shimizu A 1996 Landauer Conductance and Nonequilibrium Noise of One-Dimensional Interacting Electron Systems *J. Phys. Soc. Japan* **65** 1162–5

[9] Kamenev A and Kohn W 2001 Landauer conductance without two chemical potentials *Phys. Rev. B - Condens. Matter Mater. Phys.* **63** 1553041–15530411

[10] Smogunov A, Dal Corso A and Tosatti E 2008 Magnetic phenomena, spin-orbit effects, and Landauer conductance in Pt nanowire contacts: Density-functional theory calculations *Phys. Rev. B - Condens. Matter Mater. Phys.* **78** 1–9

[11] Papp E, Jelenfi D P, Veszeli M T and Vattay G 2019 A landauer formula for bioelectronic applications *Biomolecules* **9** 1–22

[12] Imry Y and Landauer R 1999 Conductance viewed as transmission *Rev. Mod. Phys.* **71** S306–12

[13] Langreth D C and Abrahams E 1981 Derivation of the Landauer conductance formula *Phys. Rev. B* **24** 2978–84

[14] Landauer R 1989 Conductance determined by transmission: Probes and

quantised constriction resistance *J. Phys. Condens. Matter* **1** 8099–110

[15] Büttiker M, Imry Y, Landauer R and Pinhas S 1985 Generalized many-channel conductance formula with application to small rings *Phys. Rev. B* **31** 6207–15

[16] Kazymyrenko K and Waintal X 2008 Knitting algorithm for calculating Green functions in quantum systems *Phys. Rev. B* **77** 115119

[17] Thorgilsson G, Viktorsson G and Erlingsson S I 2014 Recursive Green's function method for multi-terminal nanostructures *J. Comput. Phys.* **261** 256–66

[18] Groth C W, Wimmer M, Akhmerov A R and Waintal X 2014 Kwant: a software package for quantum transport *New J. Phys.* **16** 063065

[19] Ramírez C and Medina-Amayo L A 2017 Scattering matrix of arbitrary tight-binding Hamiltonians *Ann. Phys. (N. Y).* **378** 303–16

[20] Ramírez C 2018 Determining Transport Properties of Complex Multiterminal Systems: S-Matrix of General Tight-Binding Periodic Leads *Ann. Phys.* **530** 1700170

[21] Ramírez C, Rodríguez M J and Gomez B D 2020 Taylor series of Landauer conductance *Phys. E Low-dimensional Syst. Nanostructures* **124** 114213

[22] Lima L R F, Dusko A and Lewenkopf C 2018 Efficient method for computing the electronic transport properties of a multiterminal system *Phys. Rev. B* **97** 165405

[23] Rodríguez M J and Ramírez C 2022 A divide-and-conquer method to improve performance in quantum transport calculations: conductance in rotated graphene nanoribbons side-contact junctions *Electron. Struct.* **4** 047001

[24] Santos T P, Lima L R F and Lewenkopf C H 2019 An order N numerical method to efficiently calculate the transport properties of large systems: An algorithm optimized for sparse linear solvers *J. Comput. Phys.* **394** 440–55

[25] Mülken O, Pernice V and Blumen A 2007 Quantum transport on small-world networks: A continuous-time quantum walk approach *Phys. Rev. E* **76** 051125

[26] Çalışkan S, Novotny M A and Cerdá J I 2007 Transport through small world networks *J. Appl. Phys.* **102** 013707

[27] López E, Carmi S, Havlin S, Buldyrev S V. and Stanley H E 2006 Anomalous electrical and frictionless flow conductance in complex networks *Phys. D Nonlinear Phenom.* **224** 69–76

[28] Scuratti F, Salazar-Rios J M, Luzio A, Kowalski S, Allard S, Jung S, Scherf U, Loi M A and Caironi M 2021 Charge Transport in High-Mobility Field-Effect Transistors Based on Inkjet Printed Random Networks of Polymer Wrapped Single-Walled Carbon Nanotubes *Adv. Funct. Mater.* **31** 2006895

[29] Shin H, Park S-J, Kang B-C and Ha T-J 2022 Comprehensive analysis of two-dimensional charge transport mechanism in thin-film transistors based on random networks of single-wall carbon nanotubes using transient measurements *Nano Res.* **15** 1524–31

[30] Erdös P and Rėnyi A 1959 On random graphs I. *Publ. Math.* **6** 290–7

[31] Watts D J and Strogatz S H 1998 Collective dynamics of 'small-world' networks *Nature* **393** 440–2

[32] Albert R and Barabasi A-L 2001 Statistical mechanics of complex networks *Rev. Mod. Phys.* **74** 47–97

[33] Byeong-Cheol Kang, Choi H-J, Park S-J and Ha T-J 2021 Wearable triboelectric nanogenerators with the reduced loss of triboelectric charges by using a hole transport layer of bar-printed single-wall carbon nanotube random networks *Energy* **233** 121196

[34] Rosa M I N and Ruzzene M 2022 Small-world disordered lattices : spectral gaps and diffusive transport

Appendix A: Transfer matrix of a square lattice

Consider the following system: A square lattice of parameter α and dimensions $N \times M$ sites, with arbitrary on-site energies and fixed hopping parameter t, that is attached to M semi-infinite periodic chains of parameter α, with null on-site energies and hopping parameter t, to the left, and M to the right; as seen in Fig. A.1. Since the lattice's parameter and the chains' parameter are equal, *i.e.*, the distance between any two first neighbors sites is α, we can set it to one, or equivalently, any distance is measured in units of α.

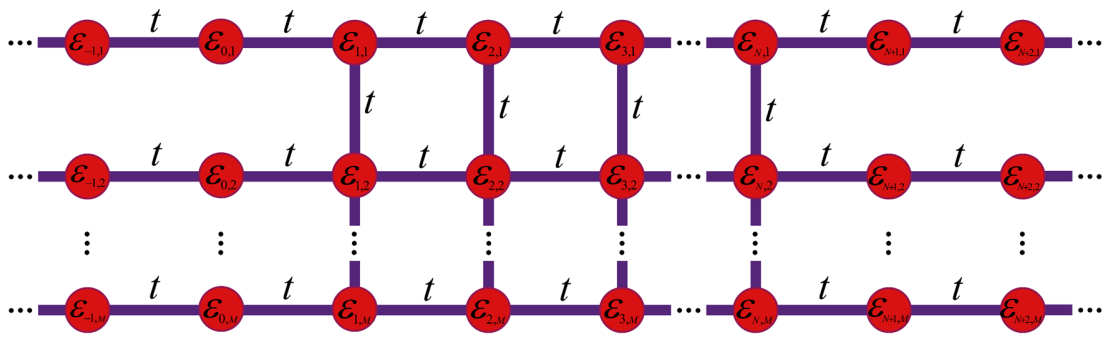

Figure A.11.- Square lattice of size $N \times M$ *attached to semi-infinite periodic chains to the left and to the right. Since it is the time-reversal case, the hopping parameters are real numbers. Also,* $\varepsilon_{n,m} = 0$ *if* $n \le 0$ *or* $n \ge N+1$.

Now, to obtain the transfer matrix of the square lattice, first notice that we can number the sites such that each one has an associated Wannier function denoted by $|n,m\rangle$, where $n \in (-\infty, \infty)$ denotes the site's column and $m \in [1, M]$ denotes the site's row. With this numeration the system is split into three parts: left chains, square lattice, and right chains. The left (right) chains consist of the sites with $n \in (-\infty, 0]$ $\left(n \in [N+1, \infty)\right)$ and any value of m, where the sites with the same m form part of the same chain.

It is well known that the eigenfunctions of a semi-infinite chain can be written in terms of left-and right-moving waves, so, we have

$$\left|\psi_m^{(\pm)}\right\rangle = \sum_n \tilde{a}_{n,m}^{(\pm)} |n,m\rangle, \tag{A.1}$$

where the superscript denotes if the wave is left-moving, $(-)$, or right-moving, $(+)$, and whose coefficients satisfy that

$$\tilde{a}_{p,m}^{(\pm)} = e^{\pm i\kappa(p-n)}\tilde{a}_{n,m}^{(\pm)}, \tag{A.2}$$

where, given that the particle has energy E,

$$E = 2t\cos(\kappa). \tag{A.3}$$

Therefore, to consider both propagation directions of the waves, we can write the eigenfunctions of the left chains as

$$\left|L_m\right\rangle = \left|\psi_m^{(+)}\right\rangle + \left|\psi_m^{(-)}\right\rangle = \sum_{n=-\infty}^{0}\left(e^{ikn}\tilde{a}_{0,m}^{(+)} + e^{-ikn}\tilde{a}_{0,m}^{(-)}\right)\left|n,m\right\rangle = \sum_{n=-\infty}^{0} a_{n,m}\left|n,m\right\rangle, \tag{A.4}$$

whereas for the right chains,

$$\left|R_m\right\rangle = \left|\psi_m^{(+)}\right\rangle + \left|\psi_m^{(-)}\right\rangle = \sum_{n=N+1}^{\infty}\left(e^{ik(n-N-1)}\tilde{a}_{N+1,m}^{(+)} + e^{-ik(n-N-1)}\tilde{a}_{N+1,m}^{(-)}\right)\left|n,m\right\rangle = \sum_{n=N+1}^{\infty} a_{n,m}\left|n,m\right\rangle. \tag{A.5}$$

To couple these chains to the square lattice, we notice that the wave amplitudes of the sites with $n=1$ ($n=N$) propagate to those with $n=0$ ($n=N+1$) via a bond of hopping parameter t. Consequently, the amplitudes in these sites differ by the same phase factor as the one inside the chains. This implies that if sites $\left|1,m\right\rangle$ and $\left|N,m\right\rangle$ have wave amplitudes $A_m^{(+)} + A_m^{(-)}$ and $\tilde{B}_m^{(+)} + \tilde{B}_m^{(-)}$ respectively, then we can write

$$\begin{aligned} a_{0,m} &= e^{-i\kappa}A_m^{(+)} + e^{i\kappa}A_m^{(-)} \\ a_{N+1,m} &= e^{i\kappa}\tilde{B}_m^{(+)} + e^{-i\kappa}\tilde{B}_m^{(-)} \end{aligned}. \tag{A.6}$$

Now, we define $B_m^{(\pm)} \equiv \tilde{B}_m^{(\mp)}$ so that the superscript states whether the waves are propagating towards the scatterer, $(+)$, or away from it, $(-)$. This is to be consistent with the interpretation handled in this work. Considering this change and defining

$$\mathbf{a}_n \equiv \begin{pmatrix} a_{n,1} \\ a_{n,2} \\ \vdots \\ a_{n,M} \end{pmatrix},\ \mathbf{A}^{(\pm)} \equiv \begin{pmatrix} A_1^{(\pm)} \\ A_2^{(\pm)} \\ \vdots \\ A_M^{(\pm)} \end{pmatrix},\ \mathbf{B}^{(\pm)} \equiv \begin{pmatrix} B_1^{(\pm)} \\ B_2^{(\pm)} \\ \vdots \\ B_M^{(\pm)} \end{pmatrix}, \tag{A.7}$$

we obtain the matrix equations

$$\begin{pmatrix}\mathbf{a}_1\\ \mathbf{a}_0\end{pmatrix}=\begin{pmatrix}\mathbf{I} & \mathbf{I}\\ e^{-i\kappa}\mathbf{I} & e^{i\kappa}\mathbf{I}\end{pmatrix}\begin{pmatrix}\mathbf{A}^{(+)}\\ \mathbf{A}^{(-)}\end{pmatrix}, \tag{A.8}$$

and

$$\begin{pmatrix}\mathbf{a}_{N+1}\\ \mathbf{a}_N\end{pmatrix}=\begin{pmatrix}e^{-i\kappa}\mathbf{I} & e^{i\kappa}\mathbf{I}\\ \mathbf{I} & \mathbf{I}\end{pmatrix}\begin{pmatrix}\mathbf{B}^{(+)}\\ \mathbf{B}^{(-)}\end{pmatrix}, \tag{A.9}$$

where $\mathbf{I}$ is the $M\times M$ identity. Notice that we can rewrite Eq. (A.9) as

$$\begin{pmatrix}\mathbf{B}^{(+)}\\ \mathbf{B}^{(-)}\end{pmatrix}=\frac{i}{2\sin(\kappa)}\begin{pmatrix}\mathbf{I} & -e^{i\kappa}\mathbf{I}\\ -\mathbf{I} & e^{-i\kappa}\mathbf{I}\end{pmatrix}\begin{pmatrix}\mathbf{a}_{N+1}\\ \mathbf{a}_N\end{pmatrix}. \tag{A.10}$$

Hence, we only need to solve the propagation of waves in the square lattice region. To do so, consider the Hamiltonian of the subsystem containing the sites with $n\in[0,N+1]$ and any m,

$$\begin{aligned}\hat{H}=\ &\sum_{n=0}^{N+1}\sum_{m=1}^{M}\varepsilon_{n,m}\left|n,m\right\rangle\left\langle n,m\right|+t\sum_{n=0}^{N}\sum_{m=1}^{M}\left[\left|n+1,m\right\rangle\left\langle n,m\right|+\left|n,m\right\rangle\left\langle n+1,m\right|\right]\\ &+t\sum_{n=1}^{N}\sum_{m=1}^{M-1}\left[\left|n,m+1\right\rangle\left\langle n,m\right|+\left|n,m\right\rangle\left\langle n,m+1\right|\right],\end{aligned} \tag{A.11}$$

and its eigenfunction

$$\left|\psi\right\rangle=\sum_{n=0}^{N+1}\sum_{m=1}^{M}a_{n,m}\left|n,m\right\rangle, \tag{A.12}$$

which has an associated eigenvalue E.

If we project the eigenvalue equation for $\left|\psi\right\rangle$ on $\left|p,1\right\rangle$, with $p\in[1,N]$, we get

$$Ea_{p,1}=\varepsilon_{p,1}a_{p,1}+ta_{p-1,1}+ta_{p+1,1}+ta_{p,2}. \tag{A.13}$$

If we do so on $\left|p,q\right\rangle$, with $p\in[1,N]$ and $q\in[2,M-1]$, we get

$$Ea_{p,q}=\varepsilon_{p,q}a_{p,q}+ta_{p-1,q}+ta_{p+1,q}+ta_{p,q-1}+ta_{p,q+1}, \tag{A.14}$$

and on $\left|p,M\right\rangle$, with $p\in[1,N]$, we get

$$Ea_{p,M}=\varepsilon_{p,M}a_{p,M}+ta_{p-1,M}+ta_{p+1,M}+ta_{p,M-1}. \tag{A.15}$$

Therefore, defining $\epsilon_{n,m}\equiv\dfrac{E-\varepsilon_{n.m}}{t}$, and using the first definition made in Eq. (A.7), we have the matrix equations

$$\mathbf{a}_p = \begin{pmatrix} \epsilon_{p-1,1} & -1 & 0 \\ -1 & \ddots & -1 \\ 0 & -1 & \epsilon_{p-1,M} \end{pmatrix} \mathbf{a}_{p-1} - \mathbf{a}_{p-2}, \tag{A.16}$$

for $p \in [2, N+1]$. Which we can rewrite as

$$\begin{pmatrix} \mathbf{a}_p \\ \mathbf{a}_{p-1} \end{pmatrix} = \begin{pmatrix} \mathbf{D}_{p-1} & -\mathbf{I} \\ \mathbf{I} & \mathbf{0} \end{pmatrix} \begin{pmatrix} \mathbf{a}_{p-1} \\ \mathbf{a}_{p-2} \end{pmatrix}, \tag{A.17}$$

where $\mathbf{I}$ and $\mathbf{0}$ are the $M \times M$ identity and null matrix respectively, and

$$\mathbf{D}_j \equiv \begin{pmatrix} \epsilon_{j,1} & -1 & 0 \\ -1 & \ddots & -1 \\ 0 & -1 & \epsilon_{j,M} \end{pmatrix}. \tag{A.18}$$

Finally, we can iterate Eq. (A.17) to obtain

$$\begin{pmatrix} \mathbf{a}_{N+1} \\ \mathbf{a}_N \end{pmatrix} = \begin{pmatrix} \mathbf{D}_N & -\mathbf{I} \\ \mathbf{I} & \mathbf{0} \end{pmatrix} \begin{pmatrix} \mathbf{D}_{N-1} & -\mathbf{I} \\ \mathbf{I} & \mathbf{0} \end{pmatrix} \cdots \begin{pmatrix} \mathbf{D}_1 & -\mathbf{I} \\ \mathbf{I} & \mathbf{0} \end{pmatrix} \begin{pmatrix} \mathbf{a}_1 \\ \mathbf{a}_0 \end{pmatrix}, \tag{A.19}$$

which allows us to relate Eqs. (A.8) and (A.10), resulting in

$$\begin{pmatrix} \mathbf{B}^{(+)} \\ \mathbf{B}^{(-)} \end{pmatrix} = \frac{i}{2\sin(\kappa)} \begin{pmatrix} \mathbf{I} & -e^{i\kappa}\mathbf{I} \\ -\mathbf{I} & e^{-i\kappa}\mathbf{I} \end{pmatrix} \begin{pmatrix} \mathbf{D}_N & -\mathbf{I} \\ \mathbf{I} & \mathbf{0} \end{pmatrix} \cdots \begin{pmatrix} \mathbf{D}_1 & -\mathbf{I} \\ \mathbf{I} & \mathbf{0} \end{pmatrix} \begin{pmatrix} \mathbf{I} & \mathbf{I} \\ e^{-i\kappa}\mathbf{I} & e^{i\kappa}\mathbf{I} \end{pmatrix} \begin{pmatrix} \mathbf{A}^{(+)} \\ \mathbf{A}^{(-)} \end{pmatrix}. \tag{A.20}$$

Hence, the transfer matrix of a $N \times M$ square lattice, with arbitrary on-site energies and fixed hopping parameter, is given by

$$\mathbf{M} = \frac{i}{2\sin(\kappa)} \begin{pmatrix} \mathbf{I} & -e^{i\kappa}\mathbf{I} \\ -\mathbf{I} & e^{-i\kappa}\mathbf{I} \end{pmatrix} \begin{pmatrix} \mathbf{D}_N & -\mathbf{I} \\ \mathbf{I} & \mathbf{0} \end{pmatrix} \cdots \begin{pmatrix} \mathbf{D}_1 & -\mathbf{I} \\ \mathbf{I} & \mathbf{0} \end{pmatrix} \begin{pmatrix} \mathbf{I} & \mathbf{I} \\ e^{-i\kappa}\mathbf{I} & e^{i\kappa}\mathbf{I} \end{pmatrix}. \tag{A.21}$$

Appendix B: S-matrix of an N+1 sites chain

Consider a chain of $N+1$ sites with null on-site energies and fixed hopping parameter t that is attached to semi-infinite periodic chains of null on-site energies and hopping parameter t_C, where the distance between any two consecutive sites is a. The Hamiltonian of such system is

$$\begin{aligned}\hat{H} = t_C \left\{ \sum_{n=-\infty}^{-1} \left[|n+1\rangle\langle n| + |n\rangle\langle n+1| \right] + \sum_{n=N}^{\infty} \left[|n+1\rangle\langle n| + |n\rangle\langle n+1| \right] \right\} \\ + t \sum_{n=0}^{N-1} \left[|n+1\rangle\langle n| + |n\rangle\langle n+1| \right],\end{aligned} \tag{B.1}$$

where $|n\rangle$ is the Wannier function of site n.

Let a_n be the wave amplitudes at the n-th site. Then, we can write the amplitudes of the first site, $n=0$, and last site, $n=N$, of the chain as

$$a_0 = A^{(+)} + A^{(-)}, \tag{B.2}$$

and

$$a_N = B^{(+)} + B^{(-)}, \tag{B.3}$$

where the superscript $(+)$ indicates the component of the amplitude corresponding to a wave traveling towards the chain, and the superscript $(-)$ does the same but for the wave traveling away from the chain.

Inside the chain, we can write the amplitude of each site in terms of right- and left-moving waves, where the amplitudes in two neighboring sites only differs by a phase factor of $e^{\pm ika}$, with the exponent's sign depending on the direction the wave is traveling and $E = 2t\cos(ka)$. Therefore, if in $|0\rangle$ we have an amplitude

$$a_0 = C + D, \tag{B.4}$$

where C (D) represents the wave amplitude corresponding to the right-moving (left-moving) wave, then the amplitude in $|N\rangle$ is given by

$$a_N = Ce^{ikaN} + De^{-ikaN}. \tag{B.5}$$

Equations (B.2) through (B.5) leave us with

$$\begin{aligned} C + D &= A^{(+)} + A^{(-)}, \\ Ce^{ikaN} + De^{-ikaN} &= B^{(+)} + B^{(-)}. \end{aligned} \tag{B.6}$$

Now, consider the eigenfunction $|\psi\rangle = \sum_n a_n |n\rangle$ associated to the energy E. Projecting its corresponding eigenvalue equation on $|0\rangle$ and $|N\rangle$ leads to

$$Ea_0 = \langle 0|\hat{H}|\psi\rangle = t_C a_{-1} + ta_1, \tag{B.7}$$

and

$$Ea_N = \langle N|\hat{H}|\psi\rangle = t_C a_{N+1} + ta_{N-1}. \tag{B.8}$$

Where, on the one hand, as mentioned before, we have the relations

$$a_1 = Ce^{ika} + De^{-ika}, \tag{B.9}$$

and

$$a_{N-1} = Ce^{ika(N-1)} + De^{-ika(N-1)}. \tag{B.10}$$

And on the other hand, we can apply the same result to sites $|0\rangle$ ($|N\rangle$) and $|-1\rangle$ ($|N+1\rangle$) with the slight difference that since the hopping between these pairs of sites is t_C, the phase factors are $e^{\pm i\kappa a}$ where $E = 2t_C \cos(\kappa a)$. This leads to

$$a_{-1} = A^{(+)}e^{-i\kappa a} + A^{(-)}e^{i\kappa a}, \tag{B.11}$$

and

$$a_{N+1} = B^{(+)}e^{-i\kappa a} + B^{(-)}e^{i\kappa a}. \tag{B.12}$$

Hence, by using Eqs. (B.2), (B.3), and (B.9) through (B.12), we have that Eqs. (B.7) and (B.8) are rewritten as

$$\begin{aligned} E\left(A^{(+)} + A^{(-)}\right) &= t_C\left(A^{(+)}e^{-i\kappa a} + A^{(-)}e^{i\kappa a}\right) + t\left(Ce^{ika} + De^{-ika}\right), \\ E\left(B^{(+)} + B^{(-)}\right) &= t_C\left(B^{(+)}e^{-i\kappa a} + B^{(-)}e^{i\kappa a}\right) + t\left(Ce^{ika(N-1)} + De^{-ika(N-1)}\right). \end{aligned} \tag{B.13}$$

Notice that

$$E - t_C e^{-i\kappa a} = t_C\left(e^{i\kappa a} + e^{-i\kappa a}\right) - t_C e^{-i\kappa a} = t_C e^{i\kappa a}, \tag{B.14}$$

and

$$-E + t_C e^{i\kappa a} = -\left(E - t_C e^{-i\kappa a}\right)^* = -t_C e^{-i\kappa a}. \tag{B.15}$$

Consequently, Eqs. (B.6) and (B.13) can be written together in a matrix equation as

$$\overbrace{\begin{pmatrix} -1 & 0 & 1 & 1 \\ 0 & -1 & e^{ikaN} & e^{-ikaN} \\ -t_C e^{-i\kappa a} & 0 & te^{ika} & te^{-ika} \\ 0 & -t_C e^{-i\kappa a} & te^{ika(N-1)} & te^{-ika(N-1)} \end{pmatrix}}^{\mathbf{M}} \begin{pmatrix} A^{(-)} \\ B^{(-)} \\ C \\ D \end{pmatrix} = \begin{pmatrix} 1 & 0 \\ 0 & 1 \\ t_C e^{i\kappa a} & 0 \\ 0 & t_C e^{i\kappa a} \end{pmatrix} \begin{pmatrix} A^{(+)} \\ B^{(+)} \end{pmatrix}. \quad \text{(B.16)}$$

To obtain the S-matrix of our system, we now need to invert the matrix $\mathbf{M}$, to do so, we compute the determinant of $\mathbf{M}$, $\det(\mathbf{M})$, and multiply de adjugate of $\mathbf{M}$, $\mathrm{adj}(\mathbf{M})$, by $1/\det(\mathbf{M})$. The determinant is given by

$$\begin{aligned} \det(\mathbf{M}) = &-\left\{-t^2\left[e^{-ika(N-2)} - e^{ika(N-2)}\right] - e^{ikaN}\left[tt_C e^{-i\kappa a}e^{-ika}\right] + e^{-ikaN}\left[tt_C e^{-i\kappa a}e^{ika}\right]\right\} \\ &+\left\{-tt_C e^{-i\kappa a}e^{-ika(N-1)} + e^{-ikaN}\left[t_C^2 e^{-2i\kappa a}\right]\right\} - \left\{-tt_C e^{-i\kappa a}e^{ika(N-1)} + e^{ikaN}\left[t_C^2 e^{-2i\kappa a}\right]\right\}, \end{aligned} \quad \text{(B.17)}$$

which reduces to

$$\det(\mathbf{M}) = -2it^2 \sin\left[ka(N-2)\right] + 4itt_C e^{-i\kappa a}\sin\left[ka(N-1)\right] - 2it_C^2 e^{-2i\kappa a}\sin\left[kaN\right]. \quad \text{(B.18)}$$

And the entries of $\mathrm{adj}(\mathbf{M})$ are given by

$$\left[\mathrm{adj}(\mathbf{M})\right]_{11} = 2it^2 \sin\left[ka(N-2)\right] - 2itt_C e^{-i\kappa a}\sin\left[ka(N-1)\right], \quad \text{(B.19)}$$

$$\left[\mathrm{adj}(\mathbf{M})\right]_{12} = -2itt_C e^{-i\kappa a}\sin\left[ka\right], \quad \text{(B.20)}$$

$$\left[\mathrm{adj}(\mathbf{M})\right]_{13} = 2it_C e^{-i\kappa a}\sin\left[kaN\right] - 2it\sin\left[ka(N-1)\right], \quad \text{(B.21)}$$

$$\left[\mathrm{adj}(\mathbf{M})\right]_{14} = 2it\sin\left[ka\right], \quad \text{(B.22)}$$

$$\left[\mathrm{adj}(\mathbf{M})\right]_{21} = -2itt_C e^{-i\kappa a}\sin\left[ka\right], \quad \text{(B.23)}$$

$$\left[\mathrm{adj}(\mathbf{M})\right]_{22} = 2it^2 \sin\left[ka(N-2)\right] - 2itt_C e^{-i\kappa a}\sin\left[ka(N-1)\right], \quad \text{(B.24)}$$

$$\left[\mathrm{adj}(\mathbf{M})\right]_{23} = 2it\sin\left[ka\right], \quad \text{(B.25)}$$

$$\left[\mathrm{adj}(\mathbf{M})\right]_{24} = 2it_C e^{-i\kappa a}\sin\left[kaN\right] - 2it\sin\left[ka(N-1)\right], \quad \text{(B.26)}$$

where we do not really need to compute any more entries because we have

$$\begin{pmatrix} A^{(-)} \\ B^{(-)} \\ C \\ D \end{pmatrix} = \frac{1}{\det(\mathbf{M})}\mathrm{adj}(\mathbf{M}) \begin{pmatrix} 1 & 0 \\ 0 & 1 \\ t_C e^{i\kappa a} & 0 \\ 0 & t_C e^{i\kappa a} \end{pmatrix} \begin{pmatrix} A^{(+)} \\ B^{(+)} \end{pmatrix}, \quad \text{(B.27)}$$

from where we conclude

$$\begin{pmatrix} A^{(-)} \\ B^{(-)} \end{pmatrix} = \begin{pmatrix} S_{11} & S_{12} \\ S_{21} & S_{22} \end{pmatrix} \begin{pmatrix} A^{(+)} \\ B^{(+)} \end{pmatrix}, \tag{B.28}$$

with

$$\begin{aligned} S_{11} &= \frac{1}{\det(\mathbf{M})}\left(\left[\mathrm{adj}(\mathbf{M})\right]_{11} + \left[\mathrm{adj}(\mathbf{M})\right]_{13} t_C e^{i\kappa a} \right), \\ S_{12} &= \frac{1}{\det(\mathbf{M})}\left(\left[\mathrm{adj}(\mathbf{M})\right]_{12} + \left[\mathrm{adj}(\mathbf{M})\right]_{14} t_C e^{i\kappa a} \right), \\ S_{21} &= \frac{1}{\det(\mathbf{M})}\left(\left[\mathrm{adj}(\mathbf{M})\right]_{21} + \left[\mathrm{adj}(\mathbf{M})\right]_{23} t_C e^{i\kappa a} \right), \\ S_{22} &= \frac{1}{\det(\mathbf{M})}\left(\left[\mathrm{adj}(\mathbf{M})\right]_{22} + \left[\mathrm{adj}(\mathbf{M})\right]_{24} t_C e^{i\kappa a} \right). \end{aligned} \tag{B.29}$$

So, after substituting Eqs. (B.18) through (B.26) in Eq. (B.29), we get that the entries of the S-matrix of a chain of parameter a and $N+1$ sites with null on-site energies and fixed hopping parameter t are given by

$$\begin{aligned} S_{11} = S_{22} &= \frac{t^2 \sin\left[ka(N-2)\right] + t_C^2 \sin\left[kaN\right] - 2tt_C \cos\left[\kappa a\right] \sin\left[ka(N-1)\right]}{-t^2 \sin\left[ka(N-2)\right] + 2tt_C e^{-i\kappa a} \sin\left[ka(N-1)\right] - t_C^2 e^{-2i\kappa a} \sin\left[kaN\right]}, \\ S_{12} = S_{21} &= \frac{2itt_C \sin\left[\kappa a\right] \sin\left[ka\right]}{-t^2 \sin\left[ka(N-2)\right] + 2tt_C e^{-i\kappa a} \sin\left[ka(N-1)\right] - t_C^2 e^{-2i\kappa a} \sin\left[kaN\right]}. \end{aligned} \tag{B.30}$$